Master's Thesis

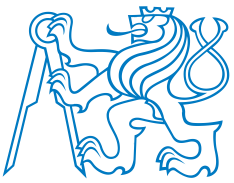

Czech Technical University in Prague

F3

Faculty of Electrical Engineering

Department of Cybernetics

Functional MRI of hypercapnia data

Bc. Lenka Vondráčková

Biomedical Informatics

May 2015

Supervisor: Mgr. Jan Petr, Ph.D., doc. Dr. Ing. Jan Kybic

Czech Technical University in Prague
Faculty of Electrical Engineering

Department of Cybernetics

DIPLOMA THESIS ASSIGNMENT

Student: Bc. Lenka V o n d r á č k o v á

Study programme: Biomedical Engineering and Informatics

Specialisation: Biomedical Informatics

Title of Diploma Thesis: Functional MRI of Hypercapnia Data

Guidelines:

1. Learn the principles of functional MR imaging and data processing.
2. Design and implement a method for evaluation of hypercapnia sequences, to distinguish between normal and pathological regions.
3. Experimentally evaluate the developed method on provided clinical data.

Bibliography/Sources:

[1] Donald W. McRobbie - MRI from Picture to Proton – 2007 Cambridge University Press
[2] Matt A. Bernstein, Kevin F. King, Xiaohong Joe Zhou - Handbook of MRI Pulse Sequences - 2004 Academic Press
[3] U. S. Yezhuvath, K. Lewis-Amezcua, R. Varghese, G. Xiao and H. Lu - On the assessment of cerebrovascular reactivity using hypercapnia BOLD MRI - 2009 NMR in biomedicine, vol. 22, no. 7, pp. 779-786
[4] William D. Penny, Karl J. Friston, John T. Ashburner,Stefan J. Kiebel, Thomas E. Nichols – Statistical Parametric Mapping: The Analysis of Functional Brain Images - 2011 Academic Press
[5] Seong-Gi Kim, Seiji Ogawa - Biophysical and physiological origins of blood oxygenation level - dependent fMRI signals - 2012 Cereb Blood Flow Metab, vol. 32, no. 7, pp.1188-1206

Diploma Thesis Supervisor: Mgr. Jan Petr, Ph.D.

Valid until: the end of the winter semester of academic year 2015/2016

L.S.

doc. Dr. Ing. Jan Kybic
Head of Department

prof. Ing. Pavel Ripka, CSc.
Dean

Prague, July 8, 2014

České vysoké učení technické v Praze
Fakulta elektrotechnická

Katedra kybernetiky

ZADÁNÍ DIPLOMOVÉ PRÁCE

Student: Bc. Lenka V o n d r á č k o v á

Studijní program: Biomedicínské inženýrství a informatika (magisterský)

Obor: Biomedicínská informatika

Název tématu: Funkční MRI hyperkapnických dat

Pokyny pro vypracování:

1. Nastudujte principy zobrazení a zpracování dat z funkční MR.
2. Navrhněte a implementujte metody pro vyhodnocování hyperkapnických sekvencí a pro rozlišení normálních a patologických oblastí.
3. Otestujte navrhnuté metody na klinických datech a vyhodnotte výsledky experimentu.

Seznam odborné literatury:

[1] Donald W. McRobbie - MRI from Picture to Proton – 2007 Cambridge University Press
[2] Matt A. Bernstein, Kevin F. King, Xiaohong Joe Zhou - Handbook of MRI Pulse Sequences - 2004 Academic Press
[3] U. S. Yezhuvath, K. Lewis-Amezcua, R. Varghese, G. Xiao and H. Lu - On the assessment of cerebrovascular reactivity using hypercapnia BOLD MRI - 2009 NMR in biomedicine, vol. 22, no. 7, pp. 779-786
[4] William D. Penny, Karl J. Friston, John T. Ashburner,Stefan J. Kiebel, Thomas E. Nichols – Statistical Parametric Mapping: The Analysis of Functional Brain Images - 2011 Academic Press
[5] Seong-Gi Kim, Seiji Ogawa - Biophysical and physiological origins of blood oxygenation level - dependent fMRI signals - 2012 Cereb Blood Flow Metab, vol. 32, no. 7, pp.1188-1206

Vedoucí diplomové práce: Mgr. Jan Petr, Ph.D.

Platnost zadání: do konce zimního semestru 2015/2016

L.S.

doc. Dr. Ing. Jan Kybic
vedoucí katedry

prof. Ing. Pavel Ripka, CSc.
děkan

V Praze dne 8. 7. 2014

Acknowledgement

I wish to express my most sincere gratitude to Mgr. Jan Petr, PhD and to doc. Dr. Ing. Jan Kybic for their patient guidance. I would like to wish my deepest thanks to Dr. Johannes Gerber and Dr. Pawel Krukowski for supervision above medical part of the study. Finally I would like to thank to Slavomir Dittrich for help with graphics in this thesis and my parents who supported me during my studies.

Declaration

Prohlašuji, že jsem předloženou práci vypracovala samostatně a že jsem uvedla veškeré použité informační zdroje v souladu s Metodickým pokynem o dodržování etických principů při přípravě vysokoškolských závěrečných prací.

V Praze dne 11.5.2015

.....

Abstrakt / Abstract

Cerebrovaskulární reaktivita (CVR) je autoregulační machanizmus udržující konstantní mozkový krevní tok a změny v CVR jsou indikátorem patologií mozkových cév. Reaktivita se dá měřit neinvazivně pomocí BOLD fMRI s hyperkapnickou stimulací. V této práci je popsán postup pro automatické zpracování dat naměřených pomocí BOLD při hyperkapnické stimulaci. Byly navrženy dvě metody a jejich výsledky jsou mezi sebou porovnány na skupině pacietů se stenózou.

První metoda (MDA) využívá jako regresor pro regresní analýzu (metoda nejmenších čtverců - MNČ) blokovou funkci s korekcí posunu konvolvonanou s hemodynamickou odezvou. Druhá metoda (DDA) využívá regresor, který by měl vykazovat lepší efektivitu v případě, že pacient není schopný přesně dodržet pokyny pro držení dechu a výdech v průběhu měření. Je založena na porovnání odezev z několika vaskulárních regionů pomocí pearsonova korelačního koeficientu (PCC), region s nejlepší korelací vůči standardní odezvě je použit jako regresor pro MNČ.

Výsledné CVR mapy byly hodnoceny skupinou lékařů (58 subjektů) a lékařským fyzikem (153 měření na 85 subjektech). Všem hodnotícím byl zamezen přístup ke klinickým datům hodnocených subjeků. Byla hodnocena celková kvalita výsledných CVR map a jejich dignostický potenciál. Kvalita byla hodnocena stupni 0-2 (0–nečitelné, 1–čitelné, 2–optimální). Metoda DDA snížila počet nečitelných případů z 12% na 3% (153 měření) a z 17% na 10% (58 subjektů). Kvalita se zlepšila v 39% případů (z 31, které byly v MDA hodnoceny 0 a 1) a 76% případů (z 42, které byly v MDA metodě hodnoceny jako 0 nebo 1). DDA poskytuje rozumné výsledky i v případech, kde standardní (MDA) metoda nestačí a je tak možným nástojem pro měření CVR v klinické praxi.

Klíčová slova: Cerebrovaskulární reakivita; hyperkapnie; zadržení dechu; BOLD; fMRI;

Cerebrovascular reactivity (CVR) is an autoregulatory mechanism that maintains constant cerebral blood flow. Impaired CVR is an indicator of pathologies of brain-feeding arteries. CVR can be assessed non-invasively using a BOLD functional MRI under hypercapnic conditions. In this thesis, we have implemented an automatic pipeline for processing of hypercapnia BOLD data using a standard method and a novel data-driven method. Their performance was compared on a group of patients with stenosis.

The standard model-driven approach (MDA) use a block function convolved with a haemodynamic response function as a regressor for CVR response evaluation. The data-driven approach (DDA) first uses Pearsons correlation coefficient (PCC) of the standard regressor with a mean responses of several selected regions to determine a region with an optimal response. The mean response of this region is then used as a regressor for the CVR analysis. This should be more efficient in case where the subject does not adhere to the breathing-protocol completely.

The CVR-maps were evaluated by a board of physicians (58 subjects) and by a medical physicist (85 subjects on 153 sessions) blinded from clinical findings. The overall image quality was scored on both methods grading from 0-2 (0 unreadable, 1 suboptimal, 2 optimal quality). The unreadable cases were reduced from 12% in MDA to 3% in DDA (153 sessions) and from 17% to 10% (58 sessions). The quality improved in 39% cases (out of 31 session that scored 0 or 1 on MDA; physicians) and in 76% cases (out of 42 session that scored 0 or 1 on MDA; physicist). DDA is a promising tool to assess CVR in clinical population. It gives reasonable results in a large number of cases where the standard analysis completely fails.

Keywords: Cerebrovascular reactivity; hypercapnia; breath holding; BOLD; fMRI;

Contents /

Tables / Figures

Chapter 1
Introduction

Today's hectic and stressful lifestyle brings many diseases of affluence. Cardiovascular diseases are the major cause of death worldwide with cerebrovascular diseases (strokes) being the cause of death in around 10% of cases[1]). The most common type of stroke is an ischemic stroke with around 80% of cases, the other 20% cases are hemorrhagic strokes [2]). Seventy percents of all ischemics strokes occur in the anterior circulation and 90% of anterior circulation strokes afflicts middle cerebral artery (MCA) and its branches [3]). MCA is the largest intracerebral vessel that supply almost the whole lateral surface of the hemispheres. This makes measurements of brain perfusion, diffusion, neuronal activity, and vessel condition an important diagnostic tool. In the past, the information about brain function was acquired solely by positron emission tomography (PET), single proton emission computed tomography (SPECT) and magnetic resonance imaging (MRI) using contrast agents.

Nowadays, there is a wide range of MRI methods for imaging the brain function and metabolism and state of vessels without the use of contrast agents. The development of new sequences and shorter acquisition times makes the functional magnetic resonance imaging (fMRI) one of the commonly used methods. The blood flow in vessels can be also measured by time-of-flight angiography. Neuronal activation can be indirectly assessed by blood oxygen level dependent (BOLD) fMRI and together with arterial spin labelling (ASL) that measures the cerebral blood flow (CBF), the rate of oxygen metabolism can be as well assessed. Recently, a new method for measuring cerebral vessel reactivity (cerebrovascular reactivity, CVR) emerged that monitors the BOLD signal changes under conditions of varying concentration of CO_2 in blood [1–2].

The basic scheme of the CVR map acquisition based on CO_2 stimulation is the following:

- BOLD signal (sensitive to level of blood oxygenation) is acquired during normal breathing.
- Change in blood CO_2 is induced by breath hold or by inhalation of CO_2 enriched gas.
- Increased concentration of CO_2 in vessels changes the vessel diameter. This leads to change in blood flow and other auto regulation mechanisms.
- Change in blood flow is observed through change in BOLD signal intensity.
- The whole process is repeated several times to make the measurement robust to noise.

The most reliable and reproducible results are obtained by automatic administration of mixture of CO_2 and air and by measuring the end-tidal pressure of CO_2. However, it is the patient comfort that is sacrificed by wearing an air-tight mask. Moreover, the necessary hardware equipment for this is not readily available on most clinical sites.

[1]) http://www.who.int/whr/2004/annex/topic/en/annex_2_en.pdf
[2]) http://www.healthknowledge.org.uk/public-health-textbook/disease-causation-diagnostic/2b-epidemiology-diseases-phs/chronic-diseases/stroke
[3]) http://emedicine.medscape.com/article/1159900-overview

Breath-holding, on the other hand is more convenient from several points of view. It increases patient comfort, speeds up the measurement by reducing technical preparations (manipulation with mask and gases). Recently, Pillai and Mikulis published a review article suggesting that availability and comfort of a simple breath-hold technique makes up for most of its limitations and is sufficient for most applications except for pre-surgical planning [3]. The disadvantage of breath-holding is that the data analysis fails in the case when the patient does not adhere completely to the breathing protocol. Delayed reaction to a command, breathing normally during a breath-hold phase, etc. can completely spoil the standard analysis. We have therefore aimed at designing a robust method for data analyzis that would deliver reliable CVR maps even when the patient's cooperation was not optimal.

This thesis has the following goals:

- Design and implement a pipeline for automatic processing of hypercapnia BOLD data. The inputs are BOLD EPI and FLAIR images in DICOM format and the output is a CVR-map overlayed over a FLAIR image normalized to the MNI template.
- Implement a standard evaluation of the vascular response assuming the block design experiment. Correct for individual delays in the patients response to commands.
- Implement a novel data-driven approach which robustly evaluates the data even when the subject is not following the measurement protocol precisely.
- Perform the analysis on a group of patients to provide an additional information for a clinical study of patients with cerebrovascular pathology.
- Compare the quality of the CVR-maps for the standard and novel analysis method and evaluate if the same regions are shown as pathological by the two methods.

Chapter 2
Background

This chapter introduces basic principles behind the study. It covers topics from MRI physics and image acquisition to physiology and metabolism. To fully understand the physiology of brain cells or the physics behind MRI we kindly refer the reader to the publications dedicated to each mentioned topic to get more detailed information and deeper description.

2.1 MRI basic

Magnetic resonance imaging is a medical imaging modality that allows imaging of soft tissues. It uses the phenomena that a nuclei in external magnetic field can absorb and re-emit electromagnetic radiation at frequency that depends on the strength of the external magnetic field. In this section, the basics of MRI are covered.

2.1.1 History

The phenomena of nuclear magnetic resonance was first described by Isidor Rabi in 1938 (awarded the Nobel prize in Physics in 1944 for his discovery). In 1946, Felix Bloch and Edward Mills Purcell discovered that a detectable signal can occur when a sample is placed in a static magnetic field and irradiated by a radio-frequency pulse with certain frequency – the Larmor frequency – and they have extended Rabi's theory to liquids and solids [4] (awarded the Nobel prize in Physics in 1952). However, it was only during the last decades of 20^{th} century that the magnetic resonance imaging was developed and the first MRI device was built.

Raymond Damar in 1971 discovered that certain mouse tumors displayed elevated relaxation times. He built with his colleagues a superconducting magnet and made a first human body image. They named the device FONAR (Field fOcussing Nuclear mAgnetic Resonance).

In 1973, Paul Lauterbur discovered that use of linear gradients in magnetic field enables to spatially encode the origin of an NMR signal. He made several measurements in the presence of gradients with different directions and reconstructed a two dimensional image of tissue proton density. For demonstration, he used tubes filled with ordinary water surrounded by heavy water. MR was the only imaging method that was able to differentiate between ordinary and heavy water. In the year of 1974, Sir Peter Mansfeld's group invented a slice-selective excitation. Later, they have also invented a rapid imaging method based on very fast gradient variations – echo planar imaging (EPI) – that is currently used in fMRI. These contributions in MR imaging development were recognized by the Nobel committee and in 2003 the Nobel Prize in Physiology or Medicine was awarded to Paul Lauterbur and Peter Mansfeld. Two Nobel Prizes in chemistry were awarded in 1991 to Richard Ernst and in 2002 to Kurt

Wüthrich. Richard Ernst's group developed a two dimensional Fourier transform imaging in 1975. This was an essential step for bringing the method to praxis because it eliminated the unsharpness of the Lauterbur's back-projection and thus lowered the demands on magnet homogeneity. He was awarded the Nobel Prize for contributions in high resolution nuclear magnetic resonance spectroscopy (MRS). Kurt Wüthrich was honored for research in MRS for determination of the three dimensional structure of biological macromolecules in solution.

The first image of a human head was acquired with MRI in 1978. And a first commercial clinical superconducting system (*Neptune* 0.15 T) was installed at Hammersmith Hospital in London. In 1984, first 1.5 T systems were introduced. However, problems with low SNR ratio, resolution and high sensitivity to noise and motion caused that MR was not common until 1990s [5–7].

During the 90s, the scanners became more frequent in clinical praxis and MRI went through a rapid development when clinical scanners with field strength of up to 7 T, stronger gradients and better coils were developed. However, the development on the software side was equally important. In the last 20 years, a big variety of new imaging sequences were introduced that allowed both faster and more precise imaging, and imaging of neuronal activation, blood flow in vessels, diffusion, perfusion as well as imaging of other tissue properties such as magnetization transfer, tissue relaxation, magnetic susceptibility, 3D spectroscopy and many more.

2.1.2 Physics

NMR is a phenomenon in which protons with non-zero spin placed in a magnetic field can absorb and re-transmit electromagnetic radiation at certain frequency. This can be used to non-invasively image proton-density and other magnetic properties of tissue. When a proton is placed in a magnetic field, the nuclear spins are polarized - aligned with (lower energy state) or against (higher energy state) the direction of the field. A static magnetic field is in literature marked as $\mathbf{B_0}$ an defined on orthogonal coordinate system x, y and z where $\mathbf{B_0}$ is parallel to the z direction. The total magnetization of all the protons is denoted as $\mathbf{M}$. The total magnetization cannot be measured directly. Instead, the $\mathbf{M}$ is diverted from the $\mathbf{B_0}$. It then starts to precess around it at Larmor frequency ω, which is proportional to the magnitude of corresponding magnetization vector (eq. (2.1)). This induces current in a receiver coil placed perpendicular to the xy plane which serves as a measure for the total magnetization $\mathbf{M}$ and is perpendicular to the z direction.

$$\omega = \gamma \cdot |\mathbf{B}|, \tag{2.1}$$

where ω_0 is Larmor frequency $[rad \cdot s^{-1}]$, γ is the gyromagnetic ratio $[rad \cdot s^{-1} \cdot T^{-1}]$ (for hydrogen H^1 $267.513 \cdot 10^6$) and B_0 main magnetic field $[T]$ [5, p. 139].

The vector $\mathbf{M}$ is diverted from the direction of $\mathbf{B_0}$ by applying an oscillating magnetic field $\mathbf{B_1}$ perpendicular to $\mathbf{B_0}$. If the frequency of oscillation of $\mathbf{B_1}$ matches Larmor frequency ω_0, the magnetization vector $\mathbf{M}$ will start rotating around the axis of $\mathbf{B_1}$ at frequency $\omega_1 = \gamma \cdot |\mathbf{B_1}|$. The $\mathbf{B_1}$ field is applied only for a short time at certain amplitude allowing to rotate the $\mathbf{M}$ vector to the transversal xy plane. The $\mathbf{B_1}$ field is emulated by an RF pulse with ω_0 frequency emitted from a coil perpendicular to $\mathbf{B_0}$.

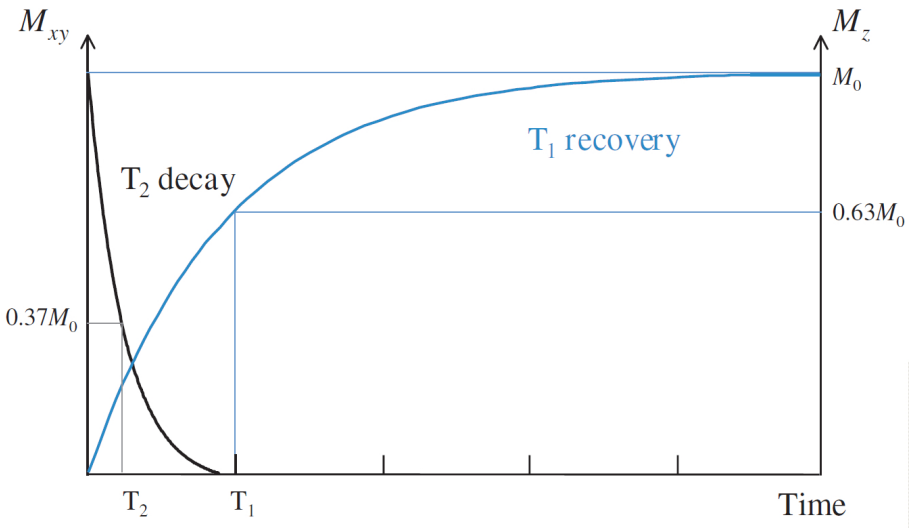

Figure 2.1. T1 and T2 decay [5].

After the $\mathbf{B_1}$ field is turned off, the flipped vector $\mathbf{M}$ continues to precess around $\mathbf{B_0}$ and can be measured.

The measurable signal ($M_{x,y}$ component of the magnetization $\mathbf{M}$) decays exponentially with time constant T2 (or T2* when the $\mathbf{B_0}$ field is not completely homogeneous) because of dephasing of its individual components. The Z-component of the magnetization returns back to equilibrium with time constant T1, see Figure 2.1 and Table 2.1. The changes in the magnetization during excitation and relaxation are fully described by Bloch equation ((9.1) see attachment). Reduced version for the case when system was initially in equilibrium and the RF pulse was 90° pulse (the flip angle is controlled by the amplitude and duration of the $\mathbf{B_1}$ RF excitation pulse) along the $+X$ axis (i.e. $M_x(0) = M_z(0) = 0$ and $M_y(0) = M_0$) the relaxation is described as:

$$M_x(t) = \mathbf{M_0} \sin(\omega t) \cdot e^{\frac{-t}{T2}} \qquad M_y(t) = \mathbf{M_0} \cos(\omega t) \cdot e^{\frac{-t}{T2}} \qquad M_z(t) = \mathbf{M_0}(1 - e^{\frac{-t}{T1}}), \quad (2.2)$$

where $\mathbf{M} = (M_x, M_y, M_z)$, ω is the Larmor frequency (2.1), and M_0 is the steady state magnetization [5].

By changing the echo-time (TE) between the excitation and measurement, and the repetition time TR between the consecutive excitations, we make the measured signal dependent on the proton density or based on the T1 and T2 properties of the tissue.

	T1 $[ms]$			T2 $[ms]$		
Tissue	0.5 T	1.5 T	3 T	0.5 T	1.5 T	3 T
WM	520	560	832	107	82	110
GM	780	1100	1331	110	92	80
CSF	-	2060	3700	-	-	-
Muscle	560	1075	898	34	33	29
Fat	132	200	382	108	-	68

Table 2.1. Relaxation times for different tissues at various field strength. Note that values were measured in-vivo from human tissues and the table is composition of values from various authors [5].

To be able to obtain 3D images of tissue, the NMR signal needs to be spatially encoded (Figure 2.2). This is done using gradient magnets, that are superimposed on the main magnetic field $\mathbf{B_0}$ and changes linearly their strength along a given direction. The first step is called slice-selection. The gradient is applied in a chosen direction (along z-axis for example) and an RF-pulse with a narrow bandwith is applied. That way we are able to rotate the $\mathbf{M}$ vector only in a given slice (depends on the strength of the gradient and bandwidth of the RF-pulse) and the rest of the volume stays intact. This way, the protons are excited and the signal measured only in a selected slice. Following the excitation, another gradient (e.g. along y-axis) is turned on for short time only, thus modifying the phase of precession depending on the spatial position on the y-axis. During the signal readout, the gradient is applied in the third ortogonal direction (e.g. along x-axis). This spatially modifies the signal frequency. This process is repeated for several different phase-encoding steps for each slice and the images are obtain by Fourier transformation of the measured signal. Please refer to the following publication for more information on MRI physics [5–6].

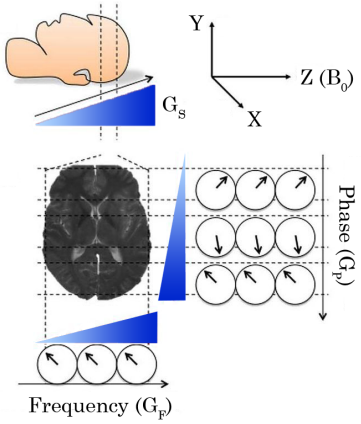

Figure 2.2. Frequence and Phase Encoding. [1])

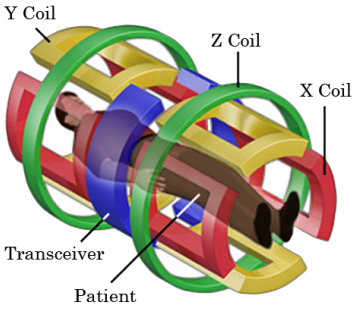

Figure 2.3. MRI Scanner Gradient Coils. [2])

2.1.3 Hardware

The basic parts of MRI scanner are the magnet, the gradients and the RF system. Together they form three kinds of magnetic fields - the main field of the scanner, the gradients and the oscillating magnetic field of RF pulses. The magnet can be permanent (up to 0.4 T) or superconducting to generate large homogeneous magnetic field (the strength can vary up to 7 T for clinical use and up to 21 T for research). Gradient coils (Figure 2.3) are usually resistive electromagnets which provides rapid and precise change of field strength in X, Y and Z direction and are used for encoding the spatial position of the NMR signal. RF system employs transmitter, coil and receiver and is used for both excitation and signal measurement. Another important parts are shim coils. Shim coils are used to dynamically adjust the homogeneity of the static magnetic field, as every subject or phantom placed in the magnet can caused inhomogeneities in the main magnetic field which then lowers the SNR or cause artifacts in the measurements [5].

2.1.4 Imaging sequences

Normally, the proton density of the brain tissue is displayed with MRI. However, with the change of imaging parameters as TR and TE (echo-time between the excitation

and measurement) we can display other properties of the tissue. By selecting a short TR, the M_z component does not fully relax to equilibrium before next excitation and the intensity of the measured signal becomes dependent on the T1-time of the tissue - such image is called T1-weighted. By prolonging TE, the difference in T2-times becomes important and such images are then T2-weighted. By using a 180° excitation pulse followed by a 90° pulse, we are able to suppress signal from tissue that has T1 time close to the delay between the 180° and 90° pulses. Such principle is used in the fluid attenuated inversion recovery (FLAIR) sequences, where signal in fluids is effectively suppressed. The fMRI images are typically acquired using so-called single-shot acquisition sequences that acquire whole image slice in a single excitation. This allows very fast imaging (order of seconds for whole brain) at the expense of decreased resolution and image deformations. With such sequences we are able to monitor changes in brain with very high time-resolution.

2.2 Brain physiology and anatomy

Brain, as other organs, needs to be surrounded by constant environment and be provided with energy supply to work properly. Energy supply and waste is carried in and out, respectively, by blood. The brain weight is around 1350 grams (approximately 2% of total body weight). However, it receives 15% of the cardiac output, 20% of total body oxygen consumption, and 25% of total body glucose utilization [8]. Glucose and oxygen are consumed for energy production and as waste product the carbon dioxide, water and other substances are produced. Most of the incoming O_2, glucose and CO_2 are consumed and produced, respectively, in the gray matter which has higher concentration of the neuronal cell bodies than the white matter which consists mostly of myelinated axons and consumes significantly less [9].

2.2.1 Neurovascular Coupling

Neurovascular coupling (NVC) is a relationship between local neural activity and changes in cerebral blood flow. It ensure that all substances such as oxygen, glucose are provided to the neurons when needed.

When a neuron communicate with another neuron, energy in the form of adenosine triphosphate (ATP) is consumed. The ATP is synthesized by oxygen and glucose metabolism. This leads to their local deficit and triggers a local increase of blood flow caused by dilatory reaction of capillaries (Figure 2.4). The exact nature of the signaling process is, however, not yet fully understood [10].

2.2.2 Cerebral blood flow

CBF is the amount of blood floating through the brain per a time unit. The total CBF in the whole brain is usually estimated as 750-1000 millilitres per minute in adults or 15% of the cardiac output. This equals to around 55 to 60 millilitres of blood per 100 grams of brain tissue per minute. CBF is almost two times higher in gray matter 75 $ml/100g/min$ than in white matter 45 $ml/100g/min$ [11].

CBF depends on a number of factors that can be broadly divided in two groups. Those affecting cerebral perfusion pressure (CPP) or those affecting the radius of cerebral vessels (for example dilatory reaction of veins to CO_2).

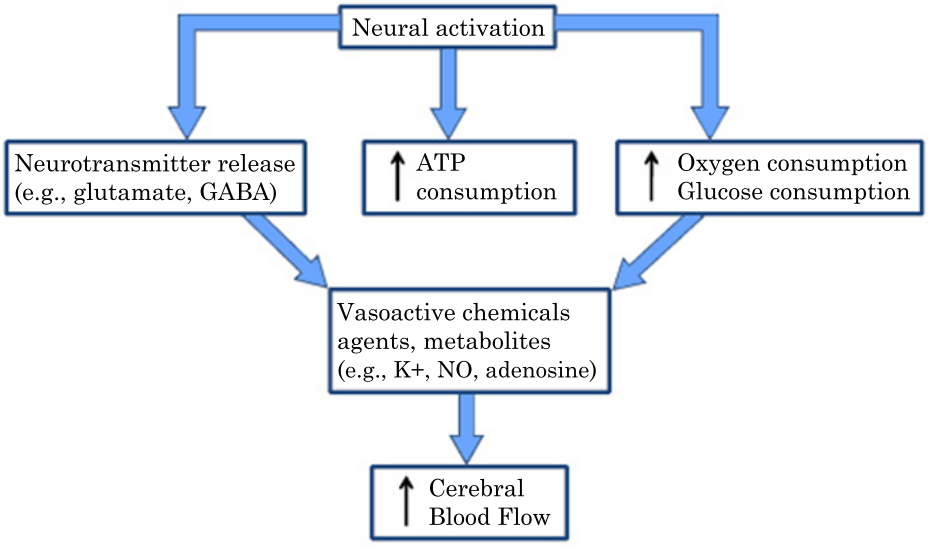

Figure 2.4. Neurovascular coupling diagram. Neural activation leads to several effects - increase in consumption of oxygen, glucose and energy stored in ATP molecules and release of transmitters. All these effects are part of signaling pattern that leads to release of vasoactive agents - dilatation of vessels and increase in blood flow. [1])

Too low CBF leads to ischemia or even tissue death. Too high CBF can raise cerebral blood volume and intracranial pressure and this state can develop intra cranial haematoma or cerebral edema. A constant flow brain in healthy brain is maintained by the vessel autoregulatory system.

CBF can be measured with transcranial doppler ultrasonography (TCD), near-infrared spectroscopy (NIRS), PET and SPECT (using dedicated tracers), or with CT or MRI using a contrast agent. Alternatively, CBF can be measured with MRI without use of contrast media - this method is called arterial spin labeling [12–14].

2.2.3 Cerebrovascular system

Superior 2/3 of brain is supplied mainly by internal carotid artery (70% of blood supply), inferior 1/3 of brain and brain stem mainly by vertebrobasilar artery (30% of blood supply). Internal carotid artery then divides mainly into middle cerebral artery (MCA) and anterior cerebral artery (ACA), vertebrobasilar artery leads blood mainly to posterior cerebral artery (PCA). MCA, ACA and PCA are connected by communicating arteries in circle of Willis (Figure 2.5). All arteries then branch out to arterioles and capillary bed (where the exchange between blood and tissue is happening) and goes back to veins trough venules. Arteries and veins are large vessels with diameter from 0.1 mm to more than 10 mm. Arterioles and venules are smaller with diameter from 10-100 μm and capillaries are the smallest with diameter around 5 μm. All vessels are lined with flattened endothelial cells and all but capillaries have smooth muscles to adjust lumen for blood flow and pressure regulation.

2.2.4 Cerebrovascular reactivity

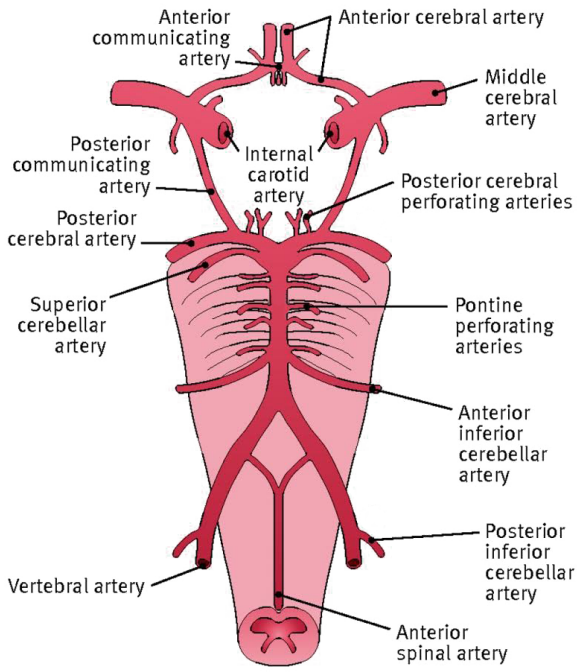

Figure 2.5. Circle of Willis diagram.[1])

CVR is described as a compensatory dilatory capacity of arterioles in the brain to the dilatatory stimulus. It falls to the category of mechanisms that affect radius of vessels and it is an important mechanism to maintain constant cerebral blood flow during changes in perfusion pressure. Reaction to different metabolic states of healthy subject is very rapid and flexible. An impaired CVR is one of the symptoms of various vessel pathologies and it has been associated with higher risk of stroke [15, 1, 16, 3].

CVR is usually categorized as normal, reduced, and paradoxical (negative) or "steal phenomenon". Negative response refers to impaired cerebrovascular reactivity of the highest degree. CVR is the key mechanism in our study and it will be described in details in chapter Cerebrovascular reactivity (3).

2.2.5 Steal phenomenon

Autoregulation reduce vascular tone to satisfy metabolic requirements and keep normal flow with up to 70% vessel blockage. However, when a vasodilatory stimulus is applied it can lead to a reduction of CBF in that region – a steal phenomenon. The explanation is the following. Vessel dilation causes CBF increase in the normal vessels. The ability of further vasodilation is limited in vessels with impaired CVR. The blood flow follows the path of least resistance and the tissue that is supplied by vessel that retain the dilatation ability "steals" the blood away from impaired area [18]. Sometimes the tissue keeps partial ability to dilate under small stimulus but when larger magnitude of stimulus is applied vasodilatory reserve is exhausted and steal phenomenon occurs. Steal can occur under the folowing circumstances [17]:

- two or more intracranial vascular beds of different vasodilatatory capacity,
- parallelly perfused from a common blood supply,
- flow capacity of the supply vessel is less than that of the vascular beds.

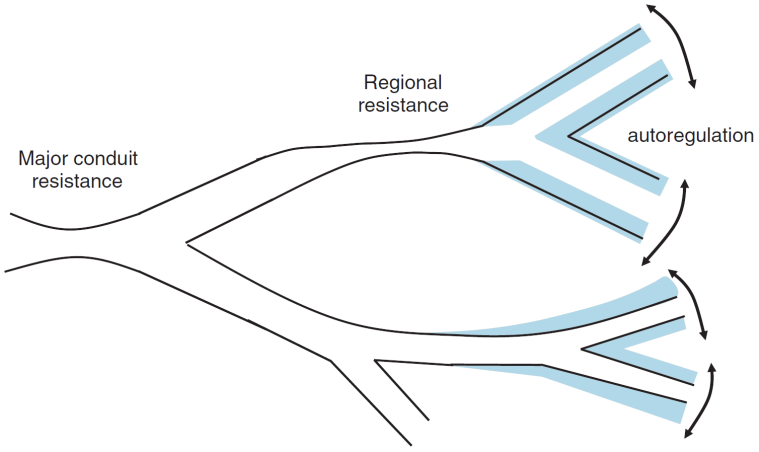

Figure 2.6. Brain vascular territory scheme. The upper branch is partially stenosed. The vasodilatory reserves of the vessels are shaded. Note, that the upper branch is already dilated to maximum while lower branch is not exhausted. A global vasodilatory stimulus will cause dilation of all vessels except of those in the upper branch that are already at the maximum of the reserve. This will cause a relative increase of CBF in the lower branch. However, the post-stimulus CBF in the upper branch will not increase as the blood is partly re-routed to the lower-branch. This phenomenon is called "vascular steal" [17].

2.3 Functional MRI

Functional magnetic resonance imaging is a method for studying brain functionality through MRI signal changes associated with neuronal activity. It became very popular especially in neurological research because of its good spatio-temporal resolution (Figure 2.7) and complete non-invasiveness.

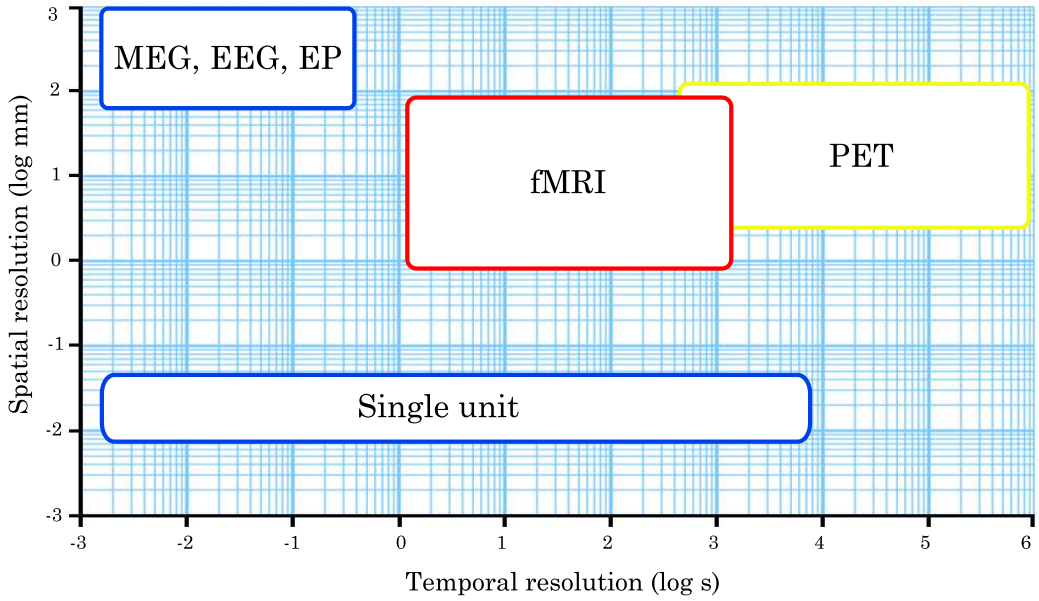

Figure 2.7. Spatio-temporal resolution of fMRI in comparison with other methods common in neurological research.

Functional MRI is used for studying brain activation induced by stimulus or event. Regions with similar pattern of changes are also studied using resting state fMRI where the subject does not perform any explicit task. The most common methods to indirectly measure the neuronal activity are blood oxygen level dependent (BOLD) that measures changes in blood oxygenation through changes in blood T2* time and arterial spin labelling that measures the tissue perfusion. Both these methods can, however, be also used to assess the vessel reactivity and the CVR of vessels through signal changes upon a vasodilatory stimulus [18].

2.3.1 ASL

ASL is a method for measuring tissue perfusion. In ASL, blood is magnetically labelled using a 180° RF pulse. The labelled blood then decreases the measurable signal in the perfused tissue. By imaging the tissue with and without prior labelling, we are able to quantify the perfusion in tissue from the difference image. The advantage compared with BOLD is the ability to quantify perfusion in standard units, while BOLD measures a combination of several effects. Disadvantage is lower signal to noise ratio and lower time resolution [18–19].

2.3.2 BOLD

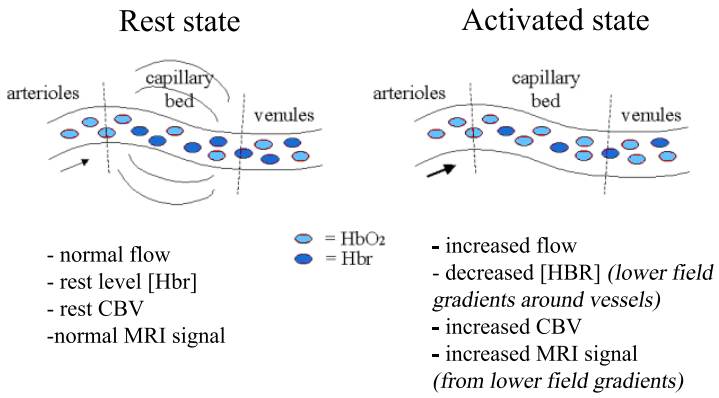

Figure 2.8. Summary of BOLD change in contrast.[1])

BOLD is the most common technique for functional MRI. Measurement is usually acquired using an EPI sequence over longer period of time. It is based on neurovascular coupling and magnetic susceptibility of blood. Basics of this method were laid down by Pauling and Coryell in 1936 when they experimented with magnetic properties of blood. They found out that magnetic susceptibilities of arterial and venous blood differ by large amount [20]. It is 20% for completely oxygenated and deoxygenated blood. These magnetic properties are caused by the presence of iron (Fe) in the haemoglobin molecule. In oxyhaemoglobin, O_2 is bound to Fe and the electron/proton values are balanced and the molecule has no charge. In deoxyhaemoglobin, the O_2 is not bound to Fe and the molecule has 2 positive charges. Ogawa made an experiment with a rat and noticed changes in signal during brain activation and measured changes in deoxyhaemoglobin and oxyhaemoglobin ratio [21]. Magnetic properties of deoxygenated blood causes inhomogeneities in magnetic field and contraction of blood T2* relaxation

time of about 1-10% [1]). At 1.5 T, oxygenated blood relaxation time is 250 ms while for deoxygenated blood it is 220 ms[22]. Posse reffered 2.1-fold increase in T2* due to visual stimulation under 20-50 mm_{Hg} end tidal partial pressure of CO_2 ($P_{ET}CO_2$). However the functional contrast was lost when $P_{ET}CO_2$ was over 70 mm_{Hg} [23]. This difference in T2* relaxation time creates the difference in contrast. See Figure 2.8 for summary [5, 24–26].

The measured BOLD intensity is highly variable because of contributions from several functional changes. Several groups have studied the problems of interscan and inter-subject variability of BOLD and proposed methods for fMRI normalisation including inhalation of medical gases, calibration task in sensorimotor, visual or auditory area and its combinations. Liau referred that BOLD have inverse dependence on baseline CBF while maximal BOLD response is independent of baseline CBF [27]. Thomason reduced variability of working memory task by 24% with breath hold calibration lasting 18 seconds [28]. However calibration in children and in adults is considered not robust enough because of more noisy response in children [29]. Cohen used inhalation method to calibrate motoric stimulation under different field strengths (1.5 T, 4 T, 7 T gradient echo and 4 T spin echo). The tests resulted in consistent results across all field strengths and sequences [30]. All previous results are in good agreement with Equation (2.3) from Kim.

The BOLD contrast is affected by changes in cerebral blood flow, cerebral blood volume, and cerebral metabolic rate of O_2 utilization. The change in venous blood oxygenation level (ΔY) is is given by:

$$\frac{\Delta Y}{1-Y} = \frac{\Delta\mathrm{CBF}/\mathrm{CBF} - \Delta\mathrm{CMRO_2}/\mathrm{CMRO_2}}{\Delta\mathrm{CBF}/\mathrm{CBF}+1}, \tag{2.3}$$

where Δ refers to the stimulus induced change. From (2.3), it can be deduced that when the relative changes of ΔCBF and $CMRO_2$ are similar then ΔY will be close to zero, otherwise the BOLD signal is correlated to CBF. [15, p. 9] If we assume that haematocrit in venous blood is the same during stimulus, then BOLD signal can be approximated as:

$$\%\mathrm{BOLD} = M\left(1 - \left(\frac{(1+\Delta\mathrm{CMRO_2}/\mathrm{CMRO_2})}{(1+\Delta\mathrm{CBF}/\mathrm{CBF}}\right)^{\beta}\left(1+\frac{\Delta\mathrm{CBV}}{\mathrm{CBV}}\right)\right), \tag{2.4}$$

where M is a constant related to baseline physiological vascular and imaging parameters. Value for β of 1.5 is commonly assumed [15]. The left term relates to the oxygen consumption versus CBF change, the right term relates to the relative CBV change, calculated from Grubb formula $(1+\Delta\mathrm{CBV}/\mathrm{CBV}) = (1+\Delta\mathrm{CBF}/\mathrm{CBF})^{\alpha}$. The value of $\alpha = 0.38$ was obtained from anaesthetized monkeys experiments and has been used for most human BOLD studies [15, p. 9].

From the previous equations,it can be seen that BOLD contrast depends mainly on cerebral blood flow. This justifies the use of BOLD as a measure for brain metabolism rate, because CBF delivers the oxygen and glucose to the centres of activation and carry away the waste products - heat and carbon dioxide.

[1]) `http://fsl.fmrib.ox.ac.uk/fmri_intro/physiology.html`

One have to be careful with interpretation of pixel intensities. MR signal intensity is a sum of contributions from multiple tissues, each with different spin density and relaxation times. This problem is even more notable with fMRI because of acquisition over time where each repetition carry anatomical and functional information. Pixel position and tissue combination vary with time because of physiological movements such as breathing, heart rate and also subject movement in scanner, and thus is impossible to attach particular pixel to precise part of tissue [15, 31].

The text written so far refers to healthy subjects only. However in case of pathological subjects with lesions, strokes, cerebrovascular disease, etc. the neurovascular coupling may not respond in expected way and this phenomena is referred to as neurovascular uncoupling. Although this usually causes true negative activation in fMRI, it can also lead to false negative activation (BOLD invisible or silent response) or false positive activation. Both are a serious problem in clinical praxis because they can lead to wrong estimation of afflicted area resulting in worse prognosis on one side and insufficient treatment on the other side [32–33, 15].

2.3.3 Hyperoxia and hypercapnia

Functional MRI data are highly variable between subjects and even in one subject between sessions. Thus calibration is recommended to reduce variance. Calibration is a process which is done before the fMRI acquisition to set the subject in a "neutral condition", to find the metabolism boundaries to have additional data about actual metabolic state. For calibration, both hypercapnia and hyperoxia can be used.

Hyperoxia is a state when a gas of higher than normal partial pressure of oxygen is inhaled, usually is considered gas mixture with 25-100% oxygen content. Basic values for oxygen are in Table 2.2. As mentioned above, oxygen is not dissolved in blood plasma as much as other gases and haemoglobin is used for transport of oxygen. In normal conditions, the arterial blood is nearly fully saturated. When the concentration of oxygen is higher, the extra oxygen is dissolved in plasma causing that venous haemoglobin is more saturated. This induces measurable changes in the concentration of oxygenated (saturated) capillary and venous blood.

"Hyperoxia method" for fMRI BOLD calibration involves $CMRO_2$ - CBF coupling and the approach is based on known oxygen delivery and change in venous blood saturation while CBF and $CMRO_2$ remains constant [34–35]. However, Chiarelli studied calibration methods based on hyperoxia, he compared vales of CBF under normoxia versus 100% hyperoxia and measured that the relative reduction of CBF is 7% [36]. In a similar study, Duong suggests that relationship between O_2 and CBF is sigmoidal and that under hypoxia condition the CBF change is exponential [37]. However, this change is small and have neglectible effect on hyperoxia calibration.

P_aO_2	Normoxia 21% O_2	Hyperoxia 100% O_2
mmHg	120.1	657.7
F%	15.8	86.5

Table 2.2. Values of end tidal partial pressure of O_2 under hyperoxia and normoxia measured by Shen and Chiarelli [34, 36] (averaged).

Hypercapnia is generally defined as a state when partial pressure in blood carbon dioxide exceeds 45 mm_{Hg}. This can be achieved by inhalation of CO_2 enriched gas or by breath hold. CO_2 is natural vasodilator and as such stimulates veins in brain to thicker their lumen to asses homoeostasis. Higher concentration of carbogen dioxide induces higher blood flow rate. In healthy subject, the reaction in whole brain is global and proportional to the vascularisation of tissue. Impaired areas, however, react differently and this can be used for assessing the state of vascular reserve. The reaction depends on stimulus length and magnitude. In CO_2 inhalation, it is the stimulus length and partial concentration. In breath hold, it depends on the phase when the breathing is stopped - end-expiration or end-inhalation and how long it is held.

In contrast to hyperoxia, hypercapnic calibration is based on CBF change due to vasodilative reaction to the CO_2 concentration and $CMRO_2$ is supposed to be constant. Because of the change in flow, impairment of cerebrovascular reactivity can be assessed using hypercapnia approach (more in the next chapter). The shape of $P_{ET}C0_2$ - CBF dependency is also sigmoidal [37].

Values of BOLD signal intensity, CBF and $CMRO_2$ under different concentration of CO_2 for hypercapnic studies are in Table 2.3 for inhalation and in Table 2.4 for breath holding.

Gas mixture	$P_{ET}CO_2$ mm_{Hg}	Fraction %	BOLD %	CBF $ml/100g/min$	$CMRO_2$ $\mu mol/100g/min$
ambient air	39.5^a	5.2	-	49 [38]	134[38]
4-5% CO_2 air	48.2^a	6.3	3 [39,40*]	80 [38]	130 [38]
7-10% CO_2 air	55^b	7.2	2.8 [41]	93.5 [23]	-
7-8% carbogen	49.5^c	6.5	5.5 [42]	-	-

Table 2.3. Values of end tidal partial pressure of CO_2 under normocapnia and hypercapnia for different gas concentrations, averaged ^{a}[23, 42, 38, 43, 40, 44–45], ^{b}[43, 23], ^{c}[16, 42], * measured with a 3 T scanner, other BOLD values with a 1.5 T scanner.

Author	Hold s	Rest s	$P_{ET}CO_2$ mm_{Hg}	BOLD %	CBF $ml/100g/min$
Kastrup^a	18	18	-	2.7	-
	30	30	-	3.2	70
	30	60	-	3.3	-
	36	48	-	2.2	62
*	40	40	-	2.7	-
Murphy[46]	20	30	45	3	-

Table 2.4. Values of end tidal partial pressure of CO_2 for different experiments with breath hold, ^{a}[39, 47–49], * breath hold after inspiration, other BH started after expiration.

Chapter 3
Cerebrovascular reactivity

CVR is a change of CBF in response to vasoactive stimulus. It is considered a sensitive indicator of brain's ability to dramatically adjust energy supply and it is a sensitive biomarker in aging studies as it can potentially reveal what goes beyond the normal decline in vessel ability to dilatation [50]. In clinical studies, CVR can predict the outcome of a bypass surgery, it reflects the severity of several diseases and CVR improvement well correlates with improvement of the disease. On the other hand CVR, is not influenced by typical risk factors for vascular diseases. Schwenrtfeger had studied changes in the CVR of healthy subjects over time (3 years) using a transcranial doppler ultrasonography (TCD) and found no significant influencing factors including gender, age and smoking [12]. In an MRI study, Fierstra evaluated smoking, diabetes, chronic obstructive pulmonary disease, asthma, hypercholesteraemia and hypertension and revealed no significant differences in CVR [51].

There are several possibilities how to assess CVR in patients. Clinically, non-invasive CVR measurements are generally performed using TCD (TCD-CVR) where changes in blood flow velocity are recorded in the middle cerebral arteries. The TCD measurements is thus insensitive to localized CVR impairment. Alternatively, BOLD-MRI measurements (henceforth termed BOLD-CVR) can be used to assessed the CVR locally [52]. There are several options how to create a vasodilatory response necessary for a CVR measurement. First is to use a vasodilatator (for example acetazolamide) which is intravenously injected and its effect is observed with imaging modality such as TCD or MRI. Effect of acetazolamide is dependent on dose and it is easily comparable between subjects and modalities. The second possibility is regulation of partial pressure of $C0_2$. The effect of acetazolamide and inhalation of CO_2 on CVR was compared by Goode. Both methods showed very good reproducibility. The advantage of CO_2 over the use of acetazolamide is its natural vasodilation and non-invasiveness [41].

The most recent model of the relationship between CBF and arterial partial pressure of CO_2 (P_aCO_2) was designed by Sobczyk. He had improved the classical model from 60s [53–55] by incorporating more recent concepts of the CBF regulation [17]:

- a sigmoidal shape of dependency of CBF on P_aCO_2,
- the vascular regions vasodilate to compensate for decreased perfusion pressure,
- vasodilation can lead to exhaustion of vasodilatory reserve, and reduced CVR,
- vasodilatory stimulus can increase CBF capacity above the flow capacity of major vessels,
- if capacity of major vessel is overreached, steal phenomena occurs [56].

The model (Figure 2.6) predicts a CBF increase as a response to a vasodilatory stimulus as depicted in Figure 3.1. However, the same stimulus leads to decrease in blood flow in a region with reduced vasodilatory reserve. This is referred to as paradoxical or negative response. The physiological effects of reduced vasodilatory reserve are altered NVC, decrease in tissue perfusion, and steal phenomenon. This makes the

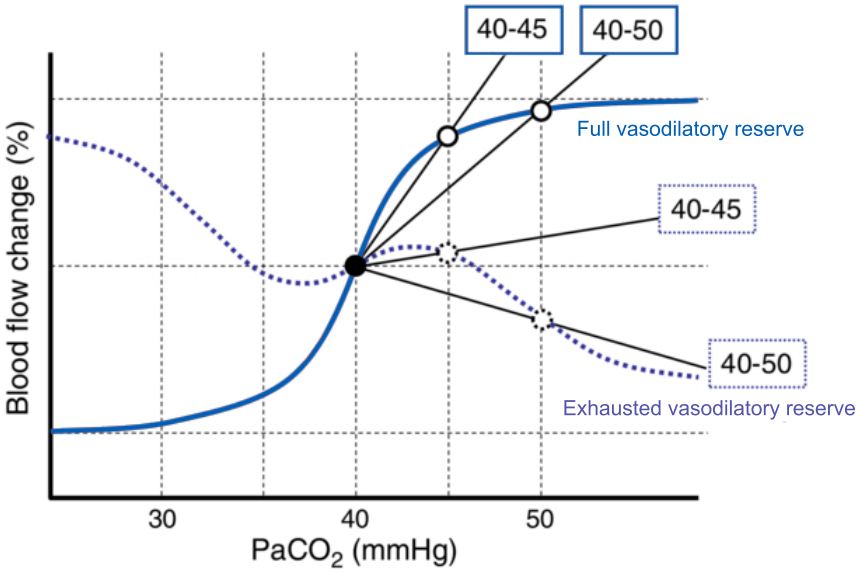

Figure 3.1. Predicted blood flow responses to P_aCO_2. The solid line depicts the sigmoidal response of normal vasodilatory reserve. The dotted line depicts the flow in a vessel with reduced vasodilatory reserve. The values on the 'Blood flow change' axis are intentionally neglected because of relative character [17].

CVR measurement a useful marker for detecting abnormalities in patients in risk of neurovascular disease [51, 57–64], cognition impairement [42] and brain tumours [65, 33]. Reduced CVR is an independent predictor for stroke [52] and may also indicate tissue exposed to episodic low-grade ischemia [59]. Altered CVR is observed in patients with Alzheimer's disease [42], cognitive impairment [42], severe depression [12], epilepsy, subarachnoid haemorrhage [60], carotid occlusion [66] or transient ischemia [47].

3.1 Hypercapnia fMRI

Blood oxygen level-dependent MRI (BOLD MRI) of hypercapnia-induced changes in cerebral blood flow is an emerging technique for mapping cerebrovascular reactivity (CVR). Higher concentration of CO_2 causes stimulus that change the lumen diameter, dramatic especially in small arteries and arterioles. Change of "pipe" diameter affects flow and volume of blood. PET studies showed that the arterial cerebral blood volume change is dominant during hyper- and hypocapnia while the venous cerebral blood volume change is minimal. Same results can be obtained with an MRI technique - VERVE[1]) [15, 37]. Hypercapnia stimulation is safe, well tolerated and technicaly feasible in clinical population with no mayor complications. However, some people may experience minor symptoms like shortness of breath, headache [50].

Commonly used methods for causing hypercapnia can be divided in two basic categories: gas inhalation (gas blender containing specific concentration of CO_2, distributed with more or less sophisticated ventilation systems) and breathing manipulation (hyperventilation, deep breathing, breath holding, etc.). Both has its pros and cons. The problem

[1]) Stefanovic B, Pike, GB (2005), Venous refocusing for volume estimation: VERVE functional magnetic imaging

of CO_2 enriched gases is the usage of a mask which is not comfortable and it is necessary to have MR-safe technique to deliver gas to the magnet room. Also, calibration of gas properties such as flow and concentration is needed. Mask has usually inbuilt gas concentration trackers and the measured curve of delivered gas or $P_{ET}CO_2$ can be used as a regressor for improved data analysis. This lowers the chance of spoiling the measurement by holding breath in incorrect moment and these results usually have good reproducibility. The BH has the advantage of being easy to implement as no dedicated hardware is needed and it can be easily performed during a routine clinical MR examination. A visual or auditory cue is used to indicate periods of breath-hold and normal breathing. Full cooperation of the subjects is, however, essential.

Most of the currently published CVR studies use a different combination of the $CO2_2$ vasoactive stimulus and settings (field strength, sequence) which makes it difficult to compare them. However, some general properties are know from other modalities or stimuli. Hypercapnia is a global stimulus affecting the whole brain, however, the largest response was measured in the cerebellum and in the visual cortex using both BH and inhalation stimuli [67, 48, 68, 45]. CVR response to both kind of stimuli is larger in gray matter and nonsignificant in white matter [45, 47] and larger in male than female [16]. Hypercapnia has a suppressive effect on metabolic rate for oxygen ($CMRO_2$) about 2-13% dependent on length of stimulus [49, 69, 38, 44], which is not problem for CVR, however, when used in combination with physical or psychical stimuli it can lead to suppression of functional contrast to such stimuli [23]. Jain used 5% CO_2 in air and the length of stimulus was 3 minutes and concluded that effect of CO_2 in $CMRO_2$ is negligible [38] in agreement with Posse [23].

3.1.1 CO_2 inhalation

CO_2 enriched gases for inhalation are usually air (5-10% CO_2, 21% O_2 and rest N_2) or carbogen (5-10% CO_2 in O_2). For both gas mixtures, a distribution mechanism is needed. This usually consist of two or three way valves to prevent rebreathing (a respiratory bag is sometimes used for rebreathing exhaled gas), a mask, and a sensor for the end tidal CO_2 tracking.

A fixed inspired fractional concentration of CO_2 does not produce a fixed $PaCO_2$. Instead, $PaCO_2$ varies both between subjects and within the same subject because it depends on the actual metabolic rate and ventilation. For this reason, it is better to use targeting (the level of CO2 in the mixture is dynamically changed in order to reach targeted concentration of $P_{ET}CO_2$) [57]. Tancerdi verified inhalation experimentally and the most reproducible results were acquired with targeting CO_2 (and O_2 in some cases) concentration in exhaled gas [70]. Spano used CO_2 targeting to assess CVR in large clinical population (294 patients, 434 measurements) and evaluated the diagnostic quality (good, diagnostic but suboptimal and nondiagnostic). They were able to generate CVR maps for 83.9% of patients. From those, 93% were classified as good, 3.3% as suboptimal and 3.3% as nondiagnostic [50].

The ideal composition of breathed gas was studied extensively. Prisman studied effect of $P_{ET}O_2$ changes on CVR during cyclic changes in $P_{ET}CO_2$ (30.4-48.8 mmHg) and $P_{ET}O_2$ (100.6-444 $mmHg$). BOLD reactivity to $P_{ET}O_2$ was smaller than to $P_{ET}CO_2$. However, BOLD reactivity to CO_2 changes can still be significantly distorted by $P_{ET}O_2$ induced changes in suggesting that $P_{ET}O_2$ should be carefully controlled [71]. Hare compared carbogen and CO_2 in air using ASL and BOLD. Both methods were correlated when using $C0_2$. However, this did not apply to carbogen stimulation. Carbogen

causes both hypercapnia and hyperoxia effects that lead to more complex response that is complicated to interpret. For this reason, Hare suggested to use CO_2 in air over carbogen for CVR mapping [19]. The length of stimulus typically varies from 1-7 minutes. Yezhuvath compared 1 and 4 min stimulus of CO_2 in air. The measured CVR values were similar in both cases suggesting that the 1 min CO_2 inhalation is sufficient for CVR mapping [45]. Moreover, shorter periods are more convenient as negative symptoms such as dizziness, shortness of breath or nausea can occur on longer periods (Spano reported 48 cases of discomfort in 434 examinations (11%) [50].

3.1.2 Breath holding

The main advantage of BH over CO_2 inhalation is easy implementation, gradual increase in CO_2 over time which leads to gradual changes in CVR response. The disadvantages are that during poor task performance the results can be misleading or false, and a presence of mild hypoxia which is considered to have negligible effect on BOLD signal [70]. No complication or side effects are associated with BH task. Contraindications for BH are dementia, language or visual impairment (because of cue) or respiratory disorders such as emphysema, chronic bronchitis because of elevated baseline CO_2 under normal condition. At Hopkins Brain Science Institute the BH protocol has been successfully implemented in approximately 95% of patients who have undergone routine clinical BOLD fMRI presurgical mapping examinations during the years 2010-2014 [3].

The main disadvantage of BH is a difficult calibration. The response is affected by several factors including the length of stimulus, metabolic rate of the patient, size of lungs, and recent ventilation history. Because of non-linear dependency of $P_{ET}CO_2$ on BH time, the effect is complicated to quantify. To obtain the absolute measure of CVR, the $P_{ET}CO_2$ have to be measured during the whole acquisition [57]. However, for clinical evaluation of the state of cerebral vessels, the absolute value of CVR is not necessary. The main information about vessel condition is carried not by the magnitude but by the direction of the BOLD change. It is expected that even a normally perfused brain can show steal phenomenon in white matter under maximal stimulus because flow resistance of arteries in white matter is 3-4 times larger than resistance of arteries in gray matter [3].

The first test in 1995 by Stillman at 4 T with as long breath hold as possible (between 1 and 2 min) showed BOLD signal intensity increase by 4-10%. This was in agreement with previous tests in TCD [72]. In 1998, Moritz reproduced similar results at 1.5 T [73]. Magon compared the effect of 9, 15 and 20 second BH. With longer BH, the variability was reduced and the voxel activation magnitude increased. However, the difference in 15 and 20 s BF was negligible [74]. In current studies, the length of BH vary between 10 to 40 s. The recommended length is between 20 - 30 seconds according to patient control/toleration limit. However, even stimulus as short as 3 s leads to measurable signal change [33]. The intra-subject variance can be further reduced by controlloing the whole breathing cycle. This was confirmed by Thomason who controled the depth of breath during rest and BH [28, 75] and by Bright who experimented with cued deep breathing which proved to be an alternative to BH [40]. However, the effect on sensitivity of steal phenomena diagnosticts is yet unknown.

3.1.3 Comparison of CO_2 inhalation and breath-holding

Big discussion is held about usage of BH or CO_2 inhalation. Both methods have strong base of studies confirming their correctness. However, there are also many studies

showing differences between the two methods [3]. In 2001, Kastrup compared using a gas blender with a 5% CO_2 inhalation and repeated breath hold for 36 seconds. Both methods induced the same BOLD changes and clarified that BHT can be employed clinically to determine CVR with fMRI [39]. Results were in agreement with previous TCD studies [76]. Bulte used ASL and BOLD to compare 30s BH and inhalation of 4% carbogen and 4% CO_2 in air. All three stimuli were used for model calibration. Results suggested, that the CO_2 in air is recommended over carbogen and BH. Both methods can lead to BOLD signal changes because in BH the level of O_2 in blood is suppressed and in carbogen elevated [77]. Tancredi employed ASL measured CBF to validate CVR using four methods: 1) CO_2 targeting; 2) administration of fixed concentration of CO_2 mixture with air; 3) BH with physiologic modelling of CO_2 accumulation; and 4) BH with hyperventilation. Methods 1-3 had consistent results in CVR percentage change while method 4 had significantly lower results. When CVR was calculated as an absolute change in CBF, methods 2 and 3 had lower value, and method 4 was dramatically lower. The outcome was that CVR should be measured avoiding hypocapnic conditions. Targeting resulted in P_ETCO_2 values that were the most consistent in linear range of CBF vs $P_{ET}CO_2$ relationships and in best fit to the CVR sigmoidal shape [70].

3.1.4 Data evaluation

BOLD-CVR with block design is evaluated similarly as standard fMRI using a generalized linear model (GLM). The block curve representing stimulus on/off is convolved with a haemodynamic response function (HRF) and a CVR statistical map is generated using regression models (GLM, least square, etc.). Recent studies adopt different regressors such as $P_{ET}CO_2$ measurement, sine-cosine curve, or a respiration response function (RRF) instead of HRF [78]. Data driven models are also used. Simon developed a method able to determine quantitative $CMRO_2$ and CBF fluctuation without a priori knowledge of temporal nature of the stimulus. He used a combination of BOLD and ASL to measure quantitative changes in CBF and $CMRO_2$ that occur in response to neural stimuli [79].

Bhogal confirmed in a hypo- to hypercapnic challenge that the sigmoidal model provides a better fit than the linear model. He also suggested that CVR is non-uniform in brain. It is not only the amplitude, but also the delay and span of response that varies in impaired tissue. This might be used in distinguishing between healthy and diseased tissue [52].

The response to stimulus is in general delayed few seconds [80]. However in BHT, the delay can be estimated more easily than in motoric or visual stimulation because the whole brain responds almost identically. Typically, a cross-correlation of regressor and response is calculated followed by shifting the model by the estimated delay. Generally, the lag had been established to be around 11 s [81]. Blockley used Fourier analysis techniques to characterize the delays of the BOLD CVR response, and showed that the frontal lobe reacted earlier (13.8 s after the start of BH) than the occipital lobe (15.2 s), the mean reaction time for GM was 14.3 s [82]. Alternatively, the temporal pattern of the signal change in purely venous structure such as superior sagittal sinus can be used directly as a regressor for analysis which eliminates the need to estimate the delay [3].

Although the HRF response is commonly used, Birn showed that the response to BH is slightly different. He designed a new model called RRF using the measured responses to BH (end exp) in several subjects and data recorded using a respiratory belt [78].

Murphy experimented with various regressors: simple block, block with time derivation, $P_{ET}CO_2$, sine-cosine and suggested that the best fit was for sine cosine or $P_{ET}CO_2$ curve [46]. Bright simulated poor task performance by taking 6 measurements in one session with variable BH lengths (10, 15 and 20 s). Additional measurement of $P_{ET}CO_2$ was recorded and used as regressor together with uniform length blocks (20 s) and time-scaled blocks. Both time scaled and uniform blocks resulted in poor repeatability, however $P_{ET}CO_2$ used as regressor resulted in excellent repeatability [83].

3.2 Patient studies

CVR is an important diagnostic marker. Hypercapnia BOLD-CVR is not yet commonly used in clinical practice. However, there were already several clinical research studies done especially in dementia, cerebrovascular disorders and tumours. Most of these studies were published by the group of Dr. Mikulis. In this Chapter, we summarize the most important applications and findings done using BOLD-CVR.

3.2.1 Moyamoya Disease

Moyamoya disease is a cerebrovascular disorder caused by blocked arteries at the base of the brain in the basal ganglia. The name ”moyamoya” means ”puff of smoke” in Japanese and it describes the look of the tangle of tiny vessels formed to compensate for the blockage. The disease primarily affects children, but it can also occur in adults. In children, the first symptom of Moyamoya disease is often a stroke, or recurrent transient ischemic attacks (commonly referred to as ”mini-strokes”). Adults most often experience a hemorrhagic stroke due to recurring blood clots in the affected brain vessels [84].

Heyn compared CVR maps from hypercapnia fMRI and angiography of 11 moyamoya patients to study relationship between CVR, steal and disease severity. Quantitative CVR showed direct correlation with impaired vascular supply in moyamoya disease [64].

Conklin compared the apparent diffusion coefficient (ADC) of normal-appearing WM (in T2-weighted images) between regions with and without steal phenomena. Measurements were done on 12 healthy volunteers and in 22 patients with Moyamoya disease and unilateral CVR impairment. Negative CVR in WM of control subjects was not associated with increase of ADC. In patients, ADC was higher in the hemisphere with negative CVR compared with ADC in the ipsilateral hemisphere and also higher than ADC in the controls. In patients, ADC was also elevated in regions with negative CVR compared with the regions with positive CVR. These findings suggest that steal phenomenon observed through negative CVR is associated with low-grade ischemic injuries before any changes are visible on T2-weighted images [59].

Fierstra noted that patients with moyamoya and stenosis had increased cortical thickness in brain areas exhibiting steal after successful revascularization. 29 subjects at an average of 11 months after surgery, cortical thickness increased in average by 5.1% in every successfully revascularized area and the CVR had also improved [57].

3.2.2 Dementia

Alzheimer’s disease (AD) is an age-related, non-reversible brain disorder that develops over a period of years. Symptoms of AD gradually lead to behavior and personality

changes, and a decline in cognitive abilities. AD ultimately leads to a severe loss of mental function. These losses are related to the worsening breakdown of the connections between certain neurons and their eventual death (as neurons cannot survive when they lose connections to other neurons). This is manifested as cortex atrophy in the affected regions [85].

Cantin used 7% carbogen mixture in patients with AD (9), and mild cognitive impairment (7) (MCI), and age-matched controls (11). Carbogen induced whole brain signal increase in all subjects. However, signal increase in AD (0.36% BOLD/$mmHg$) and MCI (0.36% BOLD/$mmHg$) patients was lower than in healthy controls (0.62% BOLD/$mmHg$). CVR impairments were predominant in posterior areas, however, the mean CVR was the best predictor of the mini-mental status examination [42].

Mikulis observed decrease in CBF in patients with arterosclerotic dementia and senile psychosis. This decrease was caused by increased vascular resistance with vascular changes preventing a "compensatory" increase in blood flow similar as in patients with advanced stenooclusive disease relationship between exhaustion and cortical thickness has been established partially reversible after surgical revascularization. Additional studies have shown that revascularization can improve cognitive decline as well as cognitive function [86].

3.2.3 Stenosis and Aneurism

A cerebral aneurysm is a weak or thin spot on a blood vessel in the brain that balloons out and fills with blood. An aneurysm can press on a nerve or surrounding tissue, and also leak or burst, which lets blood spill into surrounding tissues (called a hemorrhage). Cerebral aneurysms can occur at any age, although they are more common in adults than in children [87].

Stenosis, refers to any condition in which a blood vessel – such as an artery – becomes abnormally narrow. In the context of stroke, "stenosis" is usually caused by atherosclerosis, a condition where a blood vessel supplying blood to the brain is narrowed due to fatty deposits, known as plaques, on the vessel's inside wall [88].

Mandell compared hypercapnia BOLD and ASL in 38 patients with stenooclusive disease to confirm that the CVR-BOLD response is directly related to changes in CBF. Hemispheric CVR was significantly correlated with CBF for both GM and WM (comparison was done for paradoxical CVR). This confirms that even in patients with stenoocclusive disease, the BOLD-CVR reflects changes in CBF [89]. In different study he suggested a method to predict the hemodynamic effect of extracranial to intracranial bypasss surgery in patients with stenooclusive disease. Group with a normal preoperative CVR demonstrated no significant change in CVR after surgery. Group with reduced CVR demonstrated a significant improvement following bypass surgery. Group with paradoxial CVR demonstrated the greatest improvement [58].

Costa studied patients at risk of delayed ischemic neurological deficit (DIND). He focused on whether CVR would detect early radiological markers of vasospasm and DIND. 5 patients with aneurysmal subarachnoid hemorrhage underwent the hypercapnia challenge for CVR mapping as soon as possible after aneurysm treatment. No patients showed a vasospasm, two patients had abnormal CVR and subsequently developed DIND, three had normal CVR of which one developed posterior circulation DIND and one developed angiographic vasospasm. Costa concluded that changes in CVR 36 h

after hemorrhage had a good spatial correlation with delayed ischemia during short term follow up [60].

Chang investigated the variability of the BHT BOLD CVR dynamics in patients with significant unilateral carotid stenosis undergoing carotid angioplasty with stenting. In the group (n=5) with poor correlation between hemispheres, defined as impaired CVR, post-stenting perfusion tended to be more significantly increased, than in group (n=12) which had similar CVR responses between either hemisphere. The BOLD signal time curves of the non-stenotic side of the MCA territory were highly correlated with the average response from a previous study in normal subjects. A collateral circulation was developing with disease progression. This manifested as a change in the temporal characteristics of the BOLD signal [61].

Poublanc studied the negative BOLD-CVR response in subjects with steno-oclusive disease. Dynamic susceptibility contrast MRI was used as the gold standard measurements of the blood arrival time. The results showed high correlation between both methods. The most compromised tissue with the longest blood arrival time had the lowest (most negative) CVR magnitude. Time differences in peak BOLD-CVR response between healthy and diseased tissue were as long as 30 s in some patients, whereas corresponding blood arrival time differences were on the order of a few seconds. These results thus support the hypothesis that negative BOLD-CVR is a result of a steal phenomenon instead of delayed arrival of blood [62].

Fierstra studied relationship between impaired CVR and seizures in 20 patients with arteriovenous malformation (AVM). AVM is an abnormal connection between arteries and veins, bypassing the capillary system and epileptic seizures are common in patients with newly diagnosed brain AVM. BOLD-CVR in brain tissue adjacent to the brain AVM can help to distinguish between patients with(10) and without(10) seizures. There is a strong correlation between impaired CVR in brain tissue surrounding the AVM in the group with the tendency for epileptic seizures. In contrast, patients without seizures did not show impaired CVR in the tissue surrounding the AVM. The overall CVR in the seizure-prone group was smaller than that observed in patients with brain AVM without seizures and in controls (12), however, it still exhibited an increase in BOLD signal in response to hypercapnia [51].

3.2.4 Tumour

Zaca employed hypercapnia CVR for presurgical mapping in patients selected for lesion resection. The goal was to maximize lesion extraction while minimising damage to surrounding tissue. This is usually done using fMRI with visual, motor, cognitive or somatosensory tasks. However, tumour vasculature responds much less vigorously to physiological stimuli than vessels in normal cerebral cortex and thus the CVR mapping is a good alternative diagnostic modality.

Pillai used BH for presurgical plannig to detected regions afflicted by low grade glioma. Glioma has neurovascular uncoupling effect, and CVR mapping is a powerful method to detect abnormal neurovascular coupling [33]. Neurovascular uncoupling can manifest as a false-negative activation on BOLD fMRI. This may result in resection of healthy part of the cortex. NVU can also cause false-positive BOLD fMRI activation causing insufficient tumor resection. For this reason, detection of NVU in tumor vicinity is important for interpreting of the BOLD-fMRI findings [3].

Chapter 4
Materials

In this Chapter, we describe what measurements were done and what patients were included in the study. The protocol was designed and all the measurements were carried out at department of Neuroradiology at University hospital Carl Gustav Carus at Technical University Dresden. The aim of study was to assess the diagnostic potential of cerebro-vascular-reserve (CVR) mapping in a group of patients using a breath-hold hypercapnia BOLD. Specifically, to investigate if the CVR impairment can predict later infarction and how does the CVR pattern change after interventional therapy.

4.1 Patient data

All examinations were performed from February 2008 till September 2010 at the Department of Neuroradiology as a part of the `CVR-Study` (Study was approved by the local Ethic Committee, decision from 11.02.2008, EK172072007).

4.1.1 Subjects

Included were the patients of the Neurology Department who had a confirmed stenosis or occlusion of an extra- or an intracranial vessel. Eligible for this study were patients who fulfilled the following criteria:

- adult age,
- ability to give an informed consent,
- diagnosis confirmed on computed tomography (CTA), magnetic resonance angiography (MRA), time of flight angiography (TOF) or in digital subtraction angiography (DSA),
- more than 50% (measured according to NASCET[1]) stenosis or occlusion of the internal carotid artery (extra- (ICA ex) or intracranial (ICA in) segments), the middle cerebral artery (MCA), the vertebral (VA) or the basilar artery (BA),
- stenosis of more than one of the extra- or intracranial arterial vessels was not an exclusion criteria, in such case a "target stenosis" was defined. Criteria for choosing the target stenosis was correlation with clinical symptoms.

Excluded were all patients who:

- were not able to give informed consent or were not willing to participate in the study,
- were pregnant,
- had implants that were not MR-compatible,
- suffered from claustrophobia,
- had poor prognosis (less than 2 years, for example due to malignancies).

[1]) North American Carotid Endarterectomy Trial, [90]

In total, 59 patients were included in the study (mean age 55.0±15.3 years, range 19-81). There were 31 men (mean age 58.0) and 28 women (mean age 51.7).

- 20 patients had extracranial stenosis, 39 intracranial,
- 8 patients had a transient ischemic attack, 34 an ischemic stroke with acute infarction in the target stenosis region,
- 17 patients did not have image findings associated with the target stenosis region. Out of that, 2 patients had a transient ischemic attack and 4 had an acute infarction in a region corresponding to a stenosis in another vessel than the one with a target stenosis,
- the target stenosis region was ICA ex (n=18), ICA in (n=11), VA ex (n=2), VA in (n=2), BA (n=3), M1 (n=21), M2 (n=2).

4.1.2 Acquisitions

A 1.5 T Siemens Sonata MRI scanner with an 8-channel head-coil was used for all measurements. The study protocol consisted of four sequences: fluid attenuated inversion recovery (FLAIR), diffusion weighted imaging (DWI), time-of-flight angiography (TFA) and hypercapnia BOLD fMRI with a breath-hold task.

The common parameters of the sequences are shown in Table 4.1

Sequence	TE *ms*	TR *ms*	matrix size *pix*	voxel size *mm*	ST *mm*	SG *mm*	slices -
FLAIR	109	9000	384×512	0.45×0.45	5	1.5	19
TFA	7	37	384×512	0.39×0.39	0.8	0	87
EPI DWI	96	3100	128×128	1.8×1.8	5	1.5	19
EPI BOLD	54	3330	384×384	3.28×3.28	4	1.2	26

Table 4.1. Sequence parameters. ST stands for slice thickness, SG is slice gap. EPI DWI stands for diffusion weighted sequence with calculation of apparent diffusion coefficient.

Hypercapnia BOLD was acquired with a block-design paradigm and a breath-holding task. Patients were commanded using a microphone to breath normally and to hold their breath. The phase of normal breathing ended with inspiration and the breath-holding phase ended with expiration. The patients were not wearing any breathing mask and the concentration of gases in the expired gases was not measured. The measurement started with normal breathing which lasted for 10 EPI scans (33.3 s). Then followed alternating phases of breath-holding (7 scans in each phase, 23.3 s) and normal breathing (14 scans, 46.6 s). In total, six breath-holding phases were acquired. Three scans with normal breathing were acquired after the last breath-holding phase.

Chapter 5
Methods

In this chapter, we describe the whole data processing pipeline (5.1 and 5.2). We summarize the common approach for hypercapnia data analysis and also introduce a novel method (5.2.2). At the end of the chapter, we describe the protocol for evaluation of the quality of results both on patients (5.3). We present here only the principal aspects of the analysis. The technical details of implementation as well as a simple manual are given in the appendix.

5.1 Preprocessing

All the analysis was performed in Matlab (The MathWorks Inc., Natick, Massachusetts). For some routines we have used the SPM8 toolbox (Wellcome Trust Centre for Neuroimaging) developed at the Functional Imaging Laboratory at University College London [91].

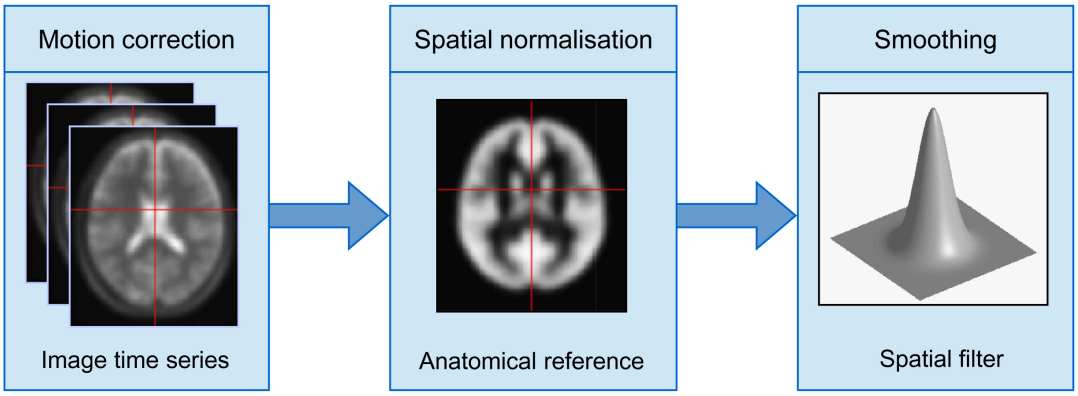

Figure 5.1. Preprocessing diagram. Preprocessing consist of motion correction, registration to standard MNI template and smoothing with gaussian kernel.

The data were downloaded from the hospital PACS system and converted from DICOM to NIFTI format using the dcm2nii program[1]). During this process, all patient information were anonymized and a unique patient ID and session ID were assigned to each dataset to allow backward identification and interpretation of clinical findings.

[1]) `http://www.mccauslandcenter.sc.edu/mricro/mricron/dcm2nii.html`

5.1.1 Motion correction

The patients in this study were mostly elderly and all had a severe cerebro-vascular disease. Given that a breath-holding task had to be performed during the fMRI measurement, slight movement during the acquisition was inevitable. As a first preprocessing step, we had therefore corrected for head motion to reduce unwanted variance in the voxel space. The Realign tool from the SPM toolbox was used for this purpose.

Realignment involved a six parameters (x,y,z translations and rotations - pitch, roll, jaw) affine transformation. The procedure looked for optimal parameters that minimize the displacements between each scan and a reference scan (first one) by using a sum-of-square differences of the intensities in the two volumes. The data were then re-sampled using the transformation with estimated parameters and B-spline interpolation. All parameters are listed in Table 5.1 [92].

Estimate		Reslice	
Parameter	Value	Parameter	Value
Quality	0.9	Which	all
Separation	4mm	Interpolation reslice	4 deg B-spline
Smoothing	5mm kernel	Wrap reslice	no
Num Passes	1	Mask	0
Interpolation	2 deg B-spline		
Wrap	no		

Table 5.1. Setup of motion correction - Realign: Estimate and Reslice.

For each subject, the maximal absolute change was calculated for all parameters and patients moving excessively were identified. As a threshold for excessive movement, we considered 5 mm in transition and 5° in rotation.

5.1.2 Spatial normalization

For several reasons, we have decided to perform spatial normalization to the MNI space. First, it compensates for different positioning of a patient on different sessions and thus allow easier evaluation of follow up studies. Second, it simplifies operations with the atlas of vascular regions. And lastly, it eases the intersubject comparison and clinical evaluation when the slices are parallel with the AC-PC plane. The Normalize tool from SPM8 was used for this purpose. The algorithm is based on minimizing the the sum of squares difference between the processed image and EPI template aligned to the MNI space using a 12-parameter affine transformation followed by a nonlinear deformation. A mean image of the whole series was used for estimation of the warping parameters [92]. The resulting voxel size was chosen as $3 \times 3 \times 5\ mm^3$.

5.1.3 Smoothing

Smoothing with Gaussian kernel has several effects. It decreases the level of noise (improves signal to noise ratio) and it renders the error distribution to be more close to normal distribution. The image resolution is reduced, however, this step is justified by the fact that hypercapnia fMRI data typically show large spatial correlations of adjacent voxels (2.4) and large regions of pathological behaviour. Smoothing was performed with a 6 mm FWHM Gaussian kernel.

Estimate		Write	
Parameter	Value	Parameter	Value
Template image	EPI.nii (SPM8)	Preserve	all
Source image smoothing	6 mm kernel	Bounding box	[-78 -112 -50; 78 76 85]
Template image smoothing	6 mm kernel		
Affine regularisation	ICBM space template	Interpolation	2 deg B-spline
Nonlinear frequency cut-off	25	Wrapping	no
Nonlinear iterations	16		
Nonlinear regularisation	1		

Table 5.2. Setup of registration to standard anatomical space - Normalise.

5.2 Data analysis

The automatic processing pipeline was implemented in Matlab. Two methods were used for data evaluation, however, most processing steps were common for both methods and it mainly differed in the choice and preprocessing of the regressors.

The first method is model-driven and it uses convolution of the block response function with haemodynamic response function (HRF) for regression analysis (in the pipeline called HRF method). The second method uses a data-driven approach and uses the region with 'Best Fit' to the expected block response as regressor (thus called BF method in the pipeline).

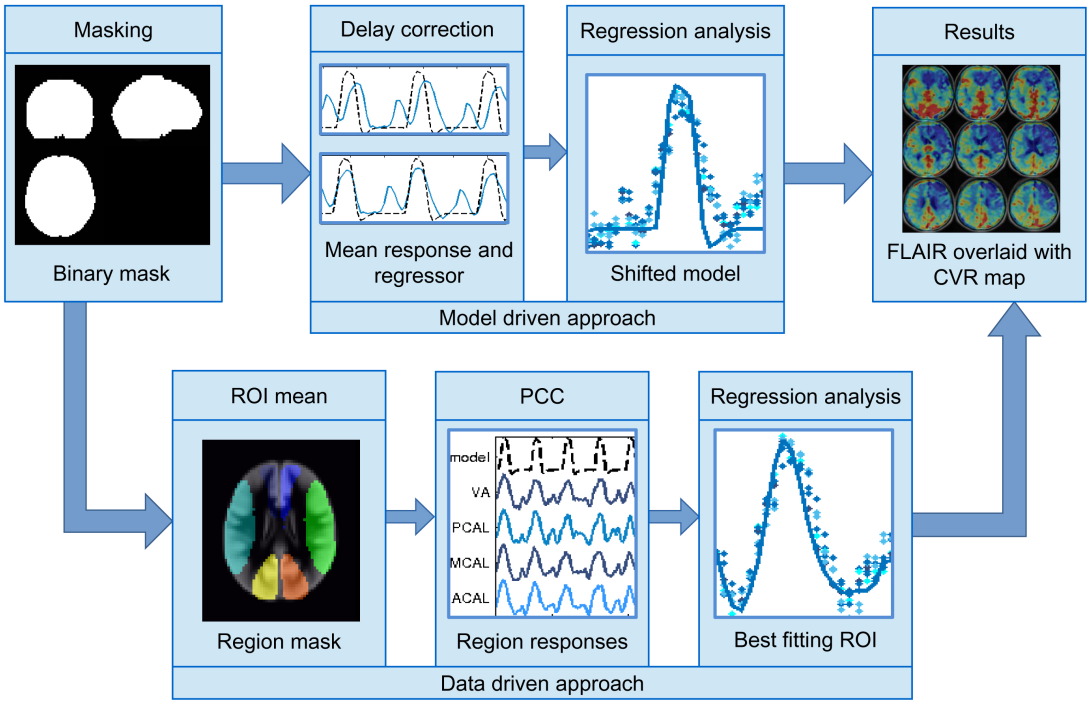

Figure 5.2. Processing diagram. The images are masked with binary mask first. Then the methods differ in regressor preparation: model-driven approach uses a model of expected response, data-driven approach uses response from region that has the most similar behaviour as the expected response. See Section 5.2.2 for details. After regression analysis, cerebrovascular reactivity maps are overlaid over anatomical image and displayed as a 'lightbox' matrix.

5.2.1 Masking

To assess only data from brain structures, the non brain structures were masked out using a binary mask of the brain from the SPM template. Additionally, the mean response of the whole brain and mean response over regions of interests (ROI) were calculated. As ROIs we used different vascular territories. It is possible to choose between mask with 7, 11 or 15 regions in the processing pipeline. For both methods we used the seven-region mask which was designed by supervising neurologist describing the localization of basic neurovascular regions. This mask consist of regions supplied by four vessels – left and right anterior cerebral artery (ACA), middle cerebral artery (MCA), posterior cerebral artery (PCA), and both vertebral arteries excluding PCA regions (VA). The mask is in the Figure 5.8. The two other maps are in the Appendix (9.1 and 9.2).

5.2.2 Regression analysis

CVR map was calculated using least squares fitting (LSQF) of a regressor function to the measured preprocessed data. The CVR response M was obtained independently in each voxel by minimizing the following ($M_{x,y,z}$, $\alpha \in \mathbb{R}$):

$$\min_{M,\alpha} \sum_t (I_{x,y,z,t} - M_{x,y,z} \cdot r_{x,y,z,t} - \alpha)^2,$$

The CVR response was thus estimated as:

$$\hat{M}_{x,y,z} = \frac{\sum_t (r_t - \mu_r) \cdot (I_{x,y,z,t} - \mu_I)}{\sum_t (r_t - \mu_r)^2}, \tag{5.1}$$

$\hat{M}$ is the resulting CVR-map, x, y, z are the image coordinates, t is time, I is the measured 4 dimensional fMRI image and r is the regressor, μ stands for mean of regressor and image, respectively, and $\hat{\alpha}$ is neglected for the clinical evaluation.

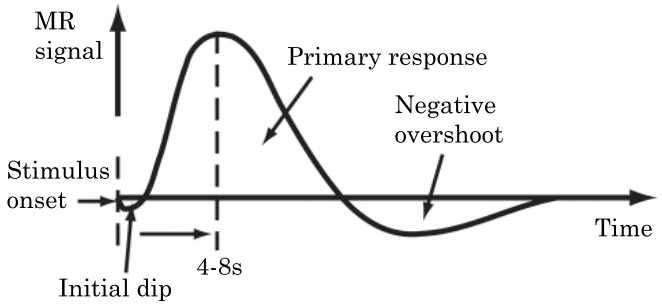

Figure 5.3. The basic haemodynamic response function[1]).

Model-driven approach

This approach uses standard block function indicating periods of normal breathing and breath-holding convolved with a HRF for regression analysis. Additionally after preprocessing and masking, the data were averaged over whole brain to obtain a mean response curve (Equation(5.2))

$$Res_t = \frac{\sum_x \sum_y \sum_z (I_{x,y,z,t} \cdot b_{x,y,z})}{\sum_x \sum_y \sum_z b_{x,y,z}}, \tag{5.2}$$

Res_t is the response for time t, x, y, z are the image coordinates, I is the measured 4 dimensional fMRI image, $b \in \{0, 1\}$ denotes the binary mask.

This was used for subject-wise delay correction (each subject has an individual delay of response to stimulus based on metabolism, previous inhalation pattern etc.). Averaged response was filtered with low-pass filter (convolution with Gaussian window length 31 scans, $\sigma = 0.8$) to remove noise and high-pass filter (Gaussian window length 31 scans, $\sigma = 10$) for drift reduction. Then it was scaled so the minimum and maximum was equal 0 and 1 (to allow easier visual comparison of regressor and mean response curves). For each patient, the cross correlation between mean response and regressor was calculated to identify the subject's delay. The ideal delay is the maximal cross correlation from regressor and mean response in time (Equation (5.3)).

$$(Res \star r)[d] \equiv \sum_{t=0}^{n} Res_t \cdot r_{[t+d]} \tag{5.3}$$

d is the delay in our case from -3 to +3, r is regressor, Res is mean response, t is time and n is the number of scans (125 in our case). The ideal lag is the $[d]$ of maximal cross correlation of mean response and regressor.

Then the regressor was shifted according to the calculated delay to fit the particular subject's response. The shifted regressor curve was then used for generating a CVR map using LSQF (Equation (5.1)).

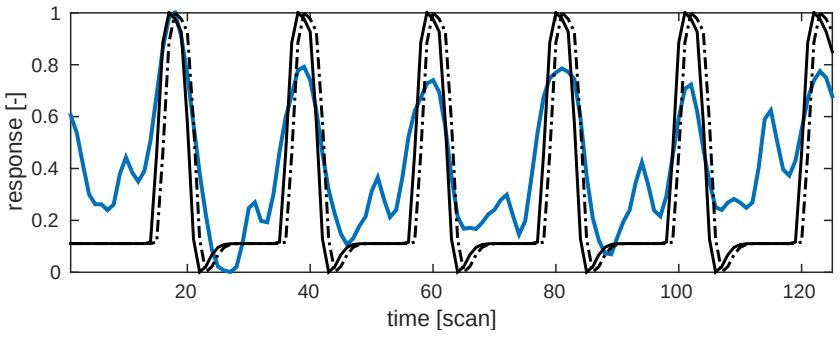

Figure 5.4. The mean curve (blue), regressor (dot-dashed black) and shifted regressor (black).

Data-driven approach

This method is novel in the field of BOLD-CVR analysis and it is the key contribution of this thesis. In this method, we assume that except for small variations, the healthy CVR response from all brain regions is similar. Moreover, we assume that each patient has at least a single large region which exhibits a normal CVR to hypercapnia. We base our assumption on the work of Goode and Chang Ting who were comparing CVR between hemispheres [41, 61]. Using the response from this region as a regressor should prove more efficient than using an expected model response in case the subject does not adhere to the breathing-protocol completely.

Similar steps as in the model-driven approach were performed first. The data were masked with a binary brain mask. Then the data were separated by ROI mask into 7 regions and mean response was calculated for each region (Equation (5.4)). Region responses were then filtered to remove drift and high-frequency noise.

$$Res_{t,k} = \frac{\sum_x \sum_y \sum_z (I_{x,y,z,t} \cdot ROI_{x,y,z,k})}{\sum_x \sum_y \sum_z ROI_{x,y,z,k}}, \tag{5.4}$$

Res is the response, x, y, z are the image coordinates, t is time, I is the measured 4 dimensional fMRI image, $k \in \{0, 1, ..., 7\}$ is the ROI identifier

Then, the Pearson's correlation coefficient (PCC) between the block-function convolved with HRF and region-wise response was calculated for each ROI, see Equation (5.5). Example of mean region responses are shown in Figure 5.5 for a subject with no CVR impairement and in Figure 5.6 for a subject with regions of impaired CVR.

$$\mathrm{PCC}_{r_t,\mathrm{ROI}_{k,t}} = \sum_t \frac{(r_t - \mu_{r_t})(\mathrm{ROI}_{k,t} - \mu_{\mathrm{ROI}_{k,t}})}{\sigma_{r_t}\sigma_{\mathrm{ROI}_{k,t}}}, \tag{5.5}$$

where μ is mean and σ stands for standard deviation, r and ROI are regressor and mean ROI response respectively, t is time (scan number) and k is ROI identifier.

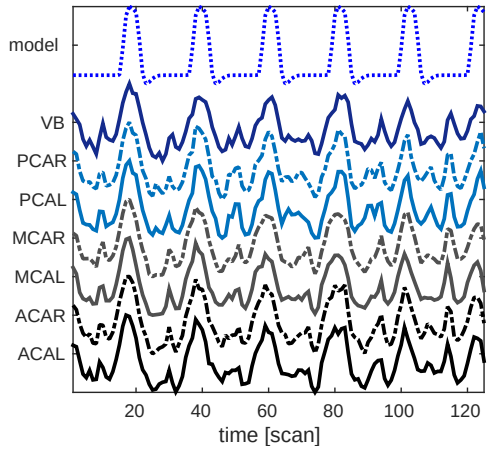

Figure 5.5. The mean responses over ROI's in a subject with no CVR impairement. The ACAR region have the largest PCC.

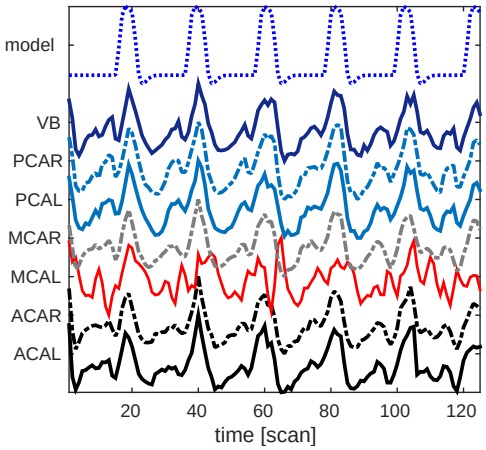

Figure 5.6. The mean regional responses in a subject with impaired CVR in the left MCA territory (red). The MCAR territory has the largest PCC.

The region with the largest PCC was considered as the reference region since it showed highest correlation with the expected healthy response. It was assumed that this region had the most normal CVR response. The mean response from this region was filtered to remove noise and drift and the amplitude was normalized similarly as in the model-driven approach. This filtered response was then used as regressor for LSQF(Equation (5.1)).

5.2.3 Results visualisation

Resulting CVR maps were overlaid over the anatomical images. Anatomical images were acquired by fluid-attenuated inversion recovery (FLAIR) or by T2 or T1 weighted spin echo sequences, in case that for particular subject FLAIR was not available. CVR-maps were displayed in 'jet' colormap with 40% opacity and they were upsampled to the same resolution as the high-resolution structural images. The result was then saved as .png containing 20 selected axial slices (position of the selected slices is shown in the Figure 5.9) ordered as 'lightbox' matrix. An example of four slices is shown in Figure 5.7.

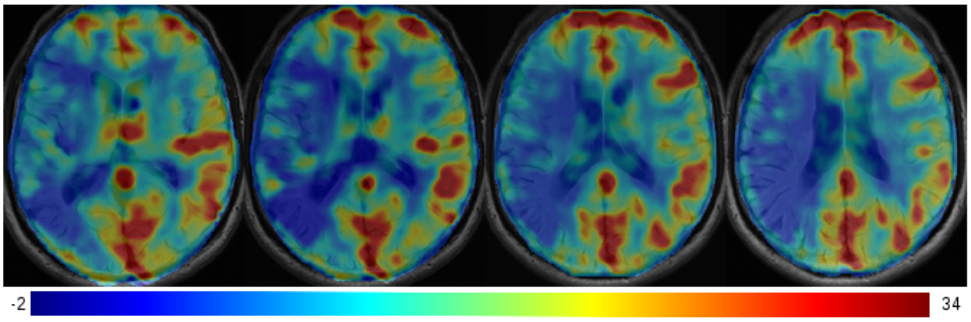

Figure 5.7. CVR map. Four slices are shown for a subject with CVR impairement in the left MCA territory. Larger CVR-response is in green-yellow to red colors (highest response) and low CVR response and paradoxical response is in blue (arbitrary units).

Combination of functional and anatomical information eases the diagnostic process in way that neurologist can link bad functional response to anatomical abnormalities in particular brain area. The processing pipeline allows selection of number (9,12,16 and 20) and position of the displayed slices (see Appendix 9.2). All slices are selected in order to contain slices at ganglionic level and slices at supra ganglionic level for evaluation by ASPECTS [1]) grading.

5.3 Method comparison

The aim of the clinical study was to evaluate the diagnostic potential of CVR induced by BH. This included evaluation of the patient reaction to therapy and comparison with changes in CVR maps. The contribution of this thesis was an implementation of a standard and an advanced method for data analysis and showing which method has the best diagnostic potential. We have therefore analyzed the results and focused only on the patients manifesting differences between the results of the methods. When the model-driven and data-driven methods gave identical clinical findings, we have

[1]) `http://www.aspectsinstroke.com/`

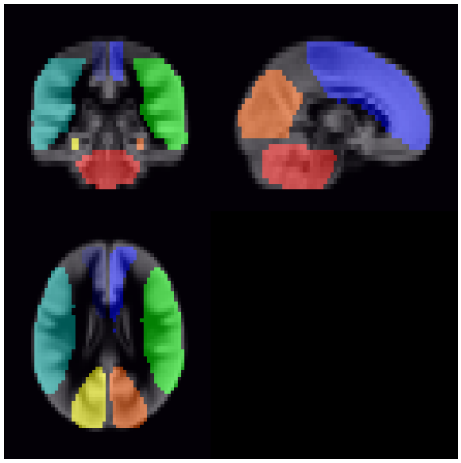

Figure 5.8. The mask with 7 basic regions of interests dark blue/blue – ACA; light-blue/green – MCA; yellow/orange – PCA; red – VA.

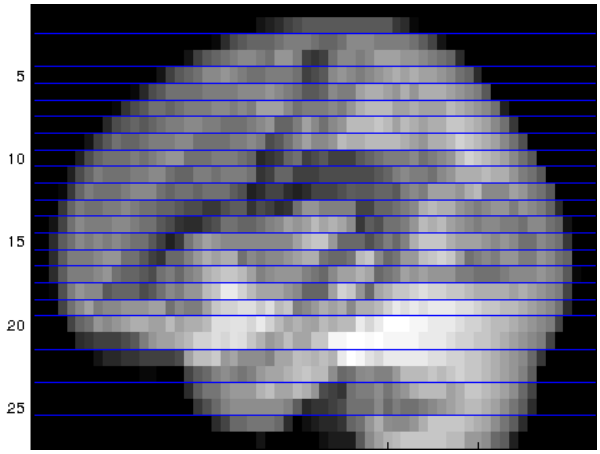

Figure 5.9. Slices selected for visualization.

considered their diagnostic potential equal and we did not further examined if this finding is correct as this will be a goal of an upcoming clinical study.

The clinical part of the study was supervised by two neuroradiologists (3 y and 10+ y of experience) who recorded the patient data and clinical findings and assessed the stenosis locations from the TOF images.

5.3.1 Criteria

First, the overall image quality was scored on grade from 0-2 (0 unreadable, 1 suboptimal, 2 optimal quality). Quality of CVR-maps was assessed based on the following criteria: sufficiently high SNR, high contrast between WM and GM, absence of CVR signal in CSF (although presence of vascular plexus had to be excluded).

Then, the pathological regions on CVR-maps were identified as showing zero or negative response, or showing response that was clearly decreased when compared to contralateral side or to overall response amplitude. The regions with reduced CVR were assessed separately in the right and left hemisphere and regions with decreased CVR were identified and marked according to the ASPECTS program. The CVR-maps that scored 0 on quality-check were not evaluated, however, the pathological regions in patients with quality 1 were assessed.

5.3.2 Readings

First, the CVR maps were evaluated by a board of 3 physicians. The board consisted of two neuroradiologists (10 y experience; 4 y experience with 10 y experience in radiology) and a neurologist (10 y experience in neurology) with stroke and neuroimaging fellowships. All the raters were blinded to the clinical findings, patient clinical history, the target stenosis region and finding from other imaging modalities. The data from the first session only from 58 patients were evaluated in two sittings. The raters were shown the CVR-map of the model-driven method only. After reaching consensus, the FLAIR image was shown and the infarct regions were identified and recorded according to ASPECTS.

More than one month later, the patients that scored 0 and 1 on model-driven quality check were re-evaluated using the BF method. Only the data-driven CVR maps were shown and the FLAIR and model-driven maps were not re-evaluated. First, all patients that scored 0 on model-driven were evaluated and then all the patients that scored 1 on model-driven. Both the quality of the data-driven CVR maps and the pathological regions according to ASPECTS were recorded.

The quality and pathological regions were assessed also by a medical physicist with 5+ y experience with neuroradiological images. The rater assessed images from all patients in all sessions (153). He was blinded to the clinical findings, patient clinical history, the target stenosis region and finding from other imaging modalities. The images were displayed in completely randomized order to blind the rater to the method, session and patient number. Only after the whole analysis was finished, the correct method, session and patient number was assigned to the findings to allow further evaluation.

5.3.3 Evaluation

After the rating, the sessions and patients numbers were assigned to appropriate score tables. The diagnostic quality of CVR maps and the difference in pathological regions was then assessed.

First, we have summarized the quality scores only. We have calculated how both methods scored in quality and we have counted the number of session in which the quality increased or decreased. Note that for the ratings by the board of medical doctors the data-driven evaluation was not available for all sessions in which model-driven scored 2 on quality.

Second, we have checked the results for differences in the findings as well. We have focused on sessions, where either the pathological regions or the quality of the images in the data-driven and model-driven methods differed. The cases where the quality and findings were identical were not considered, because we were primarily interested in comparison of model-driven and data-driven analysis in terms of better diagnostics and not in the overall evaluation of suitability of hypercapnia BOLD for clinical use. If the findings for both methods were different we have done the following to assess which of the findings are closer to reality (most important are first):

- In one of the other sessions acquired for the same patient, both methods scored 2 and had identical findings – these findings were considered as ground truth. It can happen for certain subjects that there are no more findings or that the regions with impaired CVR are smaller in later session as an effect of treatment. This was taken into account.
- The findings corresponded with the location of infarct (assessed as hyperintensity in FLAIR images in the readings by the board of physicians).
- The findings corresponded to the primary or secondary stenosis (assessed from the TOF images by the physicians supervising the study).

For certain subjects it was, however, not possible to objectively decide which method offers better results while there was only one session obtained, there was no pathological findings in the latter sessions, or the stenosis or infarct region did not correspond to the results of neither of the methods. The comparison thus led to the following cases:

- **Improved findings** – model-driven and data-driven methods differ in the pathological regions found on the CVR map. One was clearly indicated as better based on the findings from other sessions or modalities.

- **Same findings** – The independent scoring of pathological regions is in complete agreement between both methods, however, the quality was scored differently. Although the reading of the better CVR map is easier and more reliable, it did not have a direct effect on the pathological region classification.
- **Undecided** – The pathological regions differ and it is not possible to decide which finding is more correct from the available information.

All the results are summarized and shown in the Table 6.1 and 6.2.

Chapter 6
Results - evaluation

In this chapter, you can find results from the preprocessing – motion correction 6.1, and processing – delay correction 6.2. And most importantly, the results from methods evaluation in quality 6.3 and diagnostic potential 6.4 assessed by both a board of physicians and a medical physicist, in this part are presented graphical outputs of several example cases.

6.1 Motion

In preprocessing step, the motion correction with 6-parameter transformation was performed with 3 parameters for transition and 3 for rotation. The criteria for excluding the subject from analysis was 5 mm for transition or 5° for rotation. Figure 6.1 shows the distribution of maximal value in both categories for all patients. The maximal transition was 3.8 mm and maximal rotation 3.7°. No subject was thus excluded from the analysis because of excessive motion.

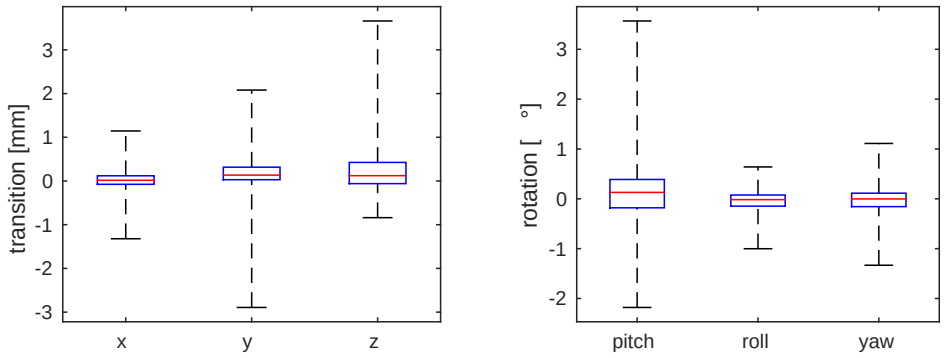

Figure 6.1. Distribution of the motion across subjects. Whiskers stand for minimum and maximum, the box denotes the first quartile and the third quartile, and red line is median.

In total, 8 sessions had translation or rotation larger than 2mm or 2°. These sessions were checked for evaluation of quality with the following results: 25% had score 2-2, 50% scored 1-2, in 12.5% the score was 2-1 and in the remaining 12.5% it was 0-0. It thus seems that larger motion is not an important factor that would prevent successfull analysis of the hypercapnia-BOLD data.

6.2 Delay

An individual delay of the response was calculated for each patient to reflect both the individual reaction time to command and the delay of BOLD response to breath-holding. This was done by calculating maximum cross-correlation of mean patient

response and the regressor, see Figure 6.2. We can observe that the delays fall into three categories: a) around 0 scan (0 *sec*)) – the true variation in the response time; b) around 9 scans (cca 30 *sec*) – this corresponds roughly to half of a breathing phase; c) around 15 scans (cca 50 *sec*) – this cluster contain only one value and corresponds to a shift by one breathing phase. The shift by a half-phase and full-phase have no physiological background and are probably caused by having too large regions with a paradoxical reponse or problems in the breathing protocol. To avoid half and whole phase shift, the estimation was limited to -3,3 scans in the processing pipeline. Resulting delays are plotted in the Figure 6.3.

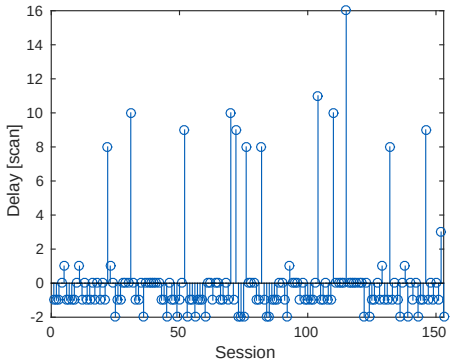

Figure 6.2. Response delays. Clusters of following values are visible in the Figure: around 0 – corresponding to true delay, around 9 – half phase shift and one value with 15 – shift by the whole breathing-phase.

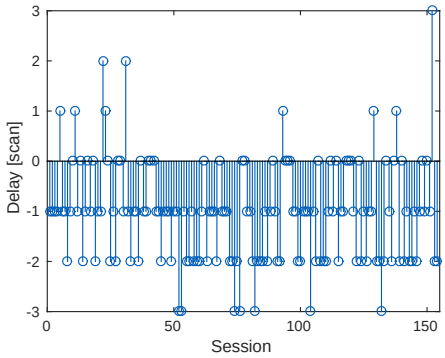

Figure 6.3. Response delays across all subjects when estimation was limited to delays between 3 and -3 scans to avoid non-physiological shifts by a half phase and full phase.

6.3 Quality evaluation

The first evaluated parameter was the overall quality of the CVR maps. Quality was scored as 0 – Unreadable (Figure 6.4), 1 – Suboptimal and 2 – Optimal quality (Figure 6.6). The scoring followed the process as described in (Section 5.3.2). Quality as well as diagnostic potential were evaluated by a board of physicians and by a medical physicist.

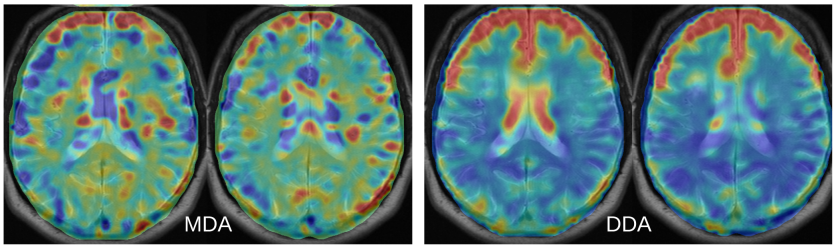

Figure 6.4. In the model driven approach, the CVR-map appear like a random noise. In DDA method, some structure is visible. However, the are artifacts on the rim around the brain and there appears to be high CVR in the ventricules - therefore the map was also evaluated as non-diagnostic. Two slices are shown for each method.

The patient in Figure 6.4 scored 0 on quality in both MDA and DDA. The poor quality of the CVR maps is probably caused by problems with breathing, see Figure 6.5.

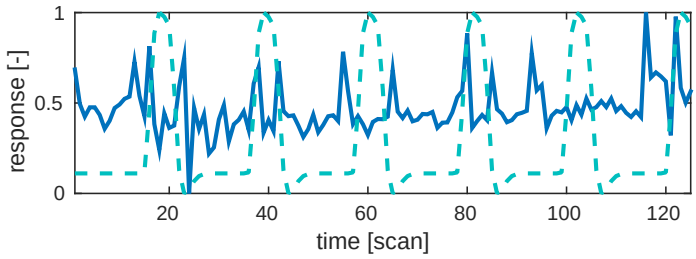

Figure 6.5. No pattern similar to the expected healthy response (dashed light blue) is visible in the mean brain response (blue full). This can be possible attributed to the subject's poor performance during the breath-holding task.

Images of different qualities in two patients are shown in Figure 6.6. In the top row, a patient with a Moyamoya disease improved quality from 0 with MDA to 2 with DDA and in the bottom row the patient with small stenosis from 1 with MDA to 2 with DDA. This patient is a typical example of breathing protocol violation, see Figure 6.7 - top. The mean response from the vascular territory supplied by the vertebral artery as assessed by DDA is shown in the Figure 6.7 - bottom. You can see that subject held breath only four times instead of six times and that the beginning and end of BH phase did not fully correspond to the model regressor. The MDA analysis therefore failed, but it was still possible to create reasonable CVR maps using the DDA method.

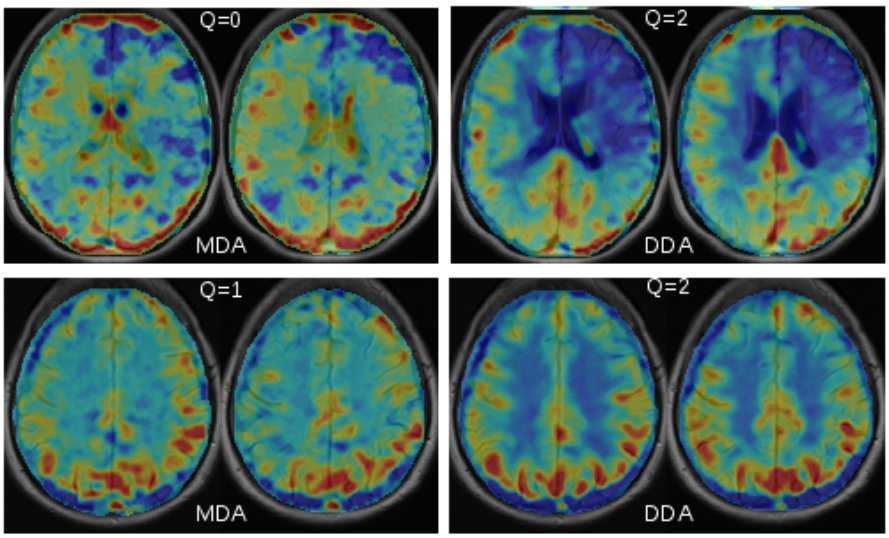

Figure 6.6. Comparison of the DDA and MDA quality for two patients (two different slices are shown for each subject). In the top row, the MDA analysis was scored with quality 0 and the CVR-map is not diagnostic (left). The DDA method was scored with quality 2 and a CVR impairment is visible in the anterior to central part of the right hemisphere. In the bottom row, the findings were identical for both MDA (quality score 1) and DDA methods (quality score 2). However, the DDA-maps show better contrast between gray and white matter and appear less noisy.

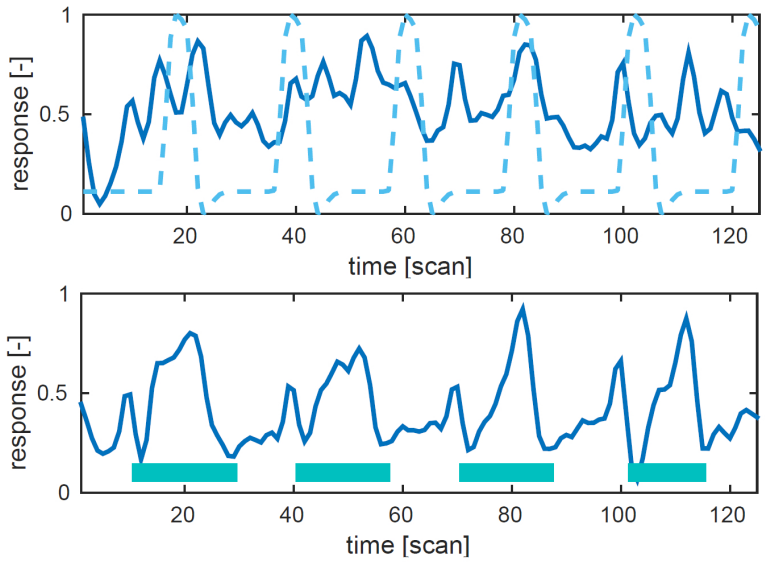

Figure 6.7. The top graph: the mean response (blue line) of the subject is very noisy and does not correlate with regressor (light blue - dashed line). The bottom graph: the mean response of the best region of the DDA method – vertebral artery territory. For convenience, the hypercapnic periods are marked manually.

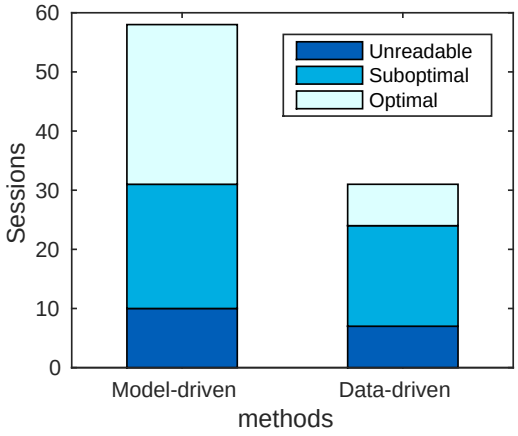

Figure 6.8. Quality evaluated by the board of physicians. For model-driven method: 27 – 'Optimal', 21 – 'Suboptimal', 10 – 'Unreadable'. In data-driven method chart are displayed only results for sessions that were 'Suboptimal' or 'Unreadable' in model-driven CVR-map. From the 31 evaluated BF-maps was 7 – 'Optimal', 17 – 'Suboptimal', 7 – 'Unreadable'.

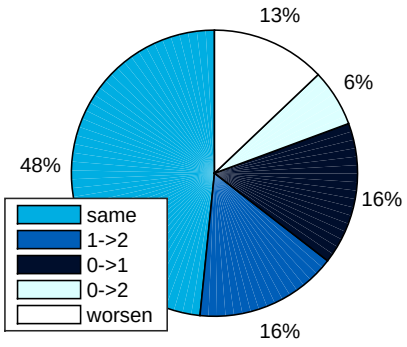

Figure 6.9. Change of quality between the model-driven and data-driven CVR-maps. Only the 31 sessions that did not scored 'Optimal' from model-driven CVR-maps were considered. 15 sessions were evaluated equally in both readings, 2 improved from 'Unreadable' to 'Optimal', 5 from 'Suboptimal' to 'Optimal' and 5 from 'Unreadable' to 'Suboptimal'. In 4 cases, the quality worsened.

6.3.1 Board – quality

From 58 subjects analysed with the model-driven method, 27 (47%) were evaluated as 'Optimal' and data-driven CVR map was not re-evaluated. 21 (36%) model-driven CVR-maps were marked as 'Suboptimal' and 10 (17%) were 'Unreadable'. Re-evaluation of the data-driven CVR-maps was done with 31 subjects of which 2 (6%) improved

quality by 2 grades, 10 (32%) improved by 1 grade, 15 (48%) had same grade, and in 4 (13%) cases the quality worsened by 1 grade. Result for quality are summarized in Figure 6.8 where all grades are counted and Figure 6.9 which considers only the results that were not marked as 'Optimal' from the model-driven CVR-map.

6.3.2 Physicist – quality

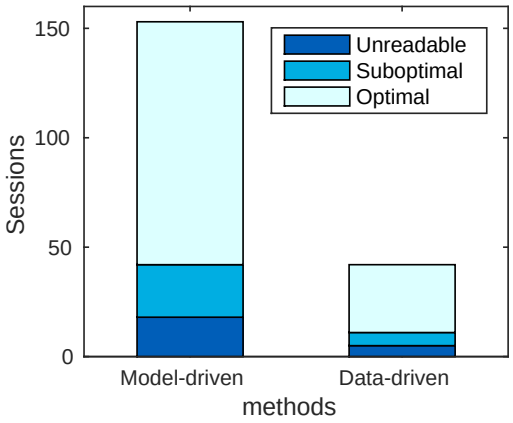

Figure 6.10. Quality evaluated by the physicist. For model-driven: 111 – 'Optimal', 24 – 'Suboptimal', 18 – 'Unreadable'. In data-driven method chart are displayed only results for sessions that were 'Suboptimal' or 'Unreadable' in model-driven CVR-map. From 42 evaluated data-driven CVR-maps was 31 – 'Optimal', 6 – 'Suboptimal', 5 – 'Unreadable'.

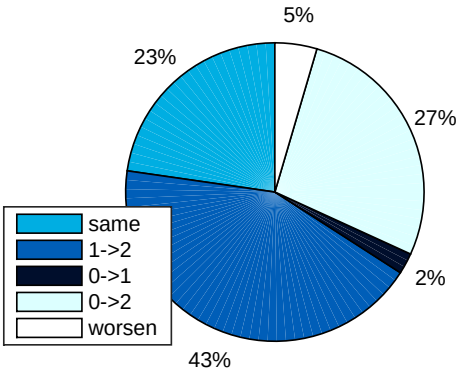

Figure 6.11. Change of quality between model-driven and data-driven CVR-maps. Only the 42 sessions which did not scored 'Optimal' from model-driven CVR-maps were considered. 10 sessions was evaluated equally in both methods, 12 improved from 'Unreadable' to 'Optimal', 19 from 'Suboptimal' to 'Optimal' and 1 from 'Unreadable' to 'Suboptimal'. In 2 cases the quality worsened.

The same quality evaluation was done by a medical physicist who evaluated all 153 sessions. The CVR-maps were randomized in both method, patient, and session identification. From 153 sessions, 111 (72%) scored 'Optimal' in model-driven method, 24 (16%) scored 'Suboptimal' and 18 (12%) 'Unreadable'. In the data-driven method, 140 (92%) sessions were 'Optimal', 8 (5%) 'Suboptimal' and 5 (3%) 'Unreadable'. From 42 session with score 0 and 1 at the first reading 12 (27%) improved quality by 2 grades, 20 (45%) improved by 1 grade, 10 (23%) had the same grade, and in 2 (5%) the quality worsened.

6.4 Evaluation of diagnostic potential

Differences in the diagnostic potential of both methods was assessed by marking the impaired regions Section 5.2.2 and then scoring the differences according to Section 5.3.3. As in the previous section, the diagnostic quality was evaluated by both board and physicist. Three states of results were achieved: 1) Improved findings – the impaired regions differ and it can be decided which is more correct – points are given to the method with better findings; 2) Same findings – the findings are same for both methods – points are given for quality; 3) Undecided – findings are different and it is not possible to clearly decide on the correct one – points are given based on quality. The results are

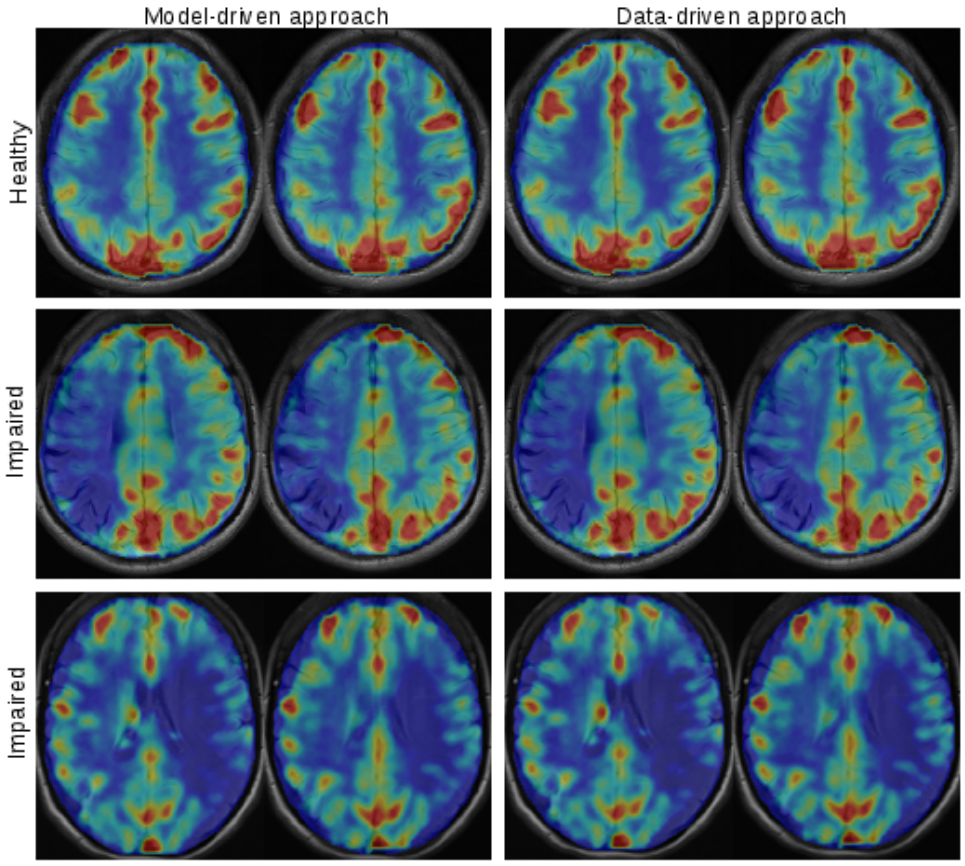

Figure 6.12. Three patients for which both methods give the same results in the same quality (two slices are shown for each subject). No CVR impairement is visible for the patient in the first row. CVR impairment in the MCA territory in the left hemisphere is visible for the patient in the middle row. This corresponds to the findings from other modalities - the patient had a stenosis in at the M1-L segment and infarct in the M4 region). Similar situation is for the patient in the last row. CVR impairment is clearly visible in the right hemisphere. The patient had a stenosis in the M1-R segment and an infarct in the M3 and M5 regions.

summarized in Tables 6.1 and 6.2. In the Figure 6.12 three patients with equal quality are shown. The first has no impairement of CVR visible. The second and third have CVR impairment in the left hemisphere and in the right hemisphere, respectively.

6.4.1 Board – diagnostic potential

In the board evaluation, only the sessions which did not score 'Optimal' in HRF maps were evaluated also for BF maps and thus allowed the method comparison. From the 31 session, in 8 cases was the diagnostic potential better in the BF method, and in 5 (3) cases in the HRF method. In 5 (7) sessions the findings were equal but differed in quality, and in 5 cases (of which 3 were unreadable in both methods) was not decided which method is better. In 10 cases, the same findings and scores were reported. In 3 cases, the results were different, however, images looked completely the same. This is marked as a number in brackets in Table 6.1 and is contributed to the error in rating.

Better method	Quality MDA-DDA	Improved findings	Same findings	Undecided	Sum	Final score
data driven	0-1	4	1	0	5	
	0-2	2	0	0	2	
	1-2	1	4	0	5	
	same	1			1	13
model driven	1-0	2(1)[a]	0	2	2(1)	
	same	4(2)	0		3(2)[b]	5(3)
none	0-0			3	0	0

Table 6.1. Results from the board of physicians; 0 – 'Unreadable', 1 – 'Suboptimal', 2 – 'Optimal'; [a,b] – images are identical, [a] in 1 case, [b] in 2 cases; In the sessions which scored as 'Optimal' for model-driven CVR-maps, the quality and diagnostic potential was not evaluated. (MDA – model-driven approach; DDA – data-driven approach)

6.4.2 Physicist – diagnostic potential

Here, we show the comparison of both methods on the data evaluated by the medical physicist. In total, there was 42 sessions that have different quality, findings or both. In 16 cases, the diagnostic potential was better in the data-driven method, in 3 cases in the model-driven method. In 13 sessions, the findings were equal, however, the quality differed. In 13 cases, it was not decided which method brings better results (5 of these case were unreadable for both methods, 3 cases had the same quality for both methods). In 5 cases, the data-driven method showed less sensitivity to the impaired CVR than the model-driven method in the follow-up sessions, and thus showing a more improvement by the treatment than the model-driven maps showed Figure 6.13. Patient underwent a stent treatment and the CVR improvement after surgery is visible in the CVR-maps. The progress is shown on three sessions, two before and one after surgery.

Better method	Quality MDA-DDA	Improved findings	Same findings	Undecided	Sum	Final score
data driven	0-1	0	0	1	1	
	0-2	6	5	1	12	
	1-2	6	7	3	16	
	same	4			4	33
model driven	1-0	0	0	0	0	
	2-0	0	0	0	0	
	2-1	1	1	0	2	
	same	7 (2)[a]			7 (2)	9 (4)
none	0-0		5			
	same			3		

Table 6.2. Results from the randomized evaluation by a medical physicist; 0 – 'Unreadable', 1 – 'Suboptimal', 2 – 'Optimal'; Unlike in the evaluation by the board of physicist, the quality and findings were available for both methods for all sessions for all patients. In 5 cases, the data-driven method showed less sensitivity to the impaired CVR than the model-driven method in the follow-up sessions, and thus showing a more improvement by the treatment than the model-driven CVR-maps showed. (MDA – model-driven approach; DDA – data-driven approach)

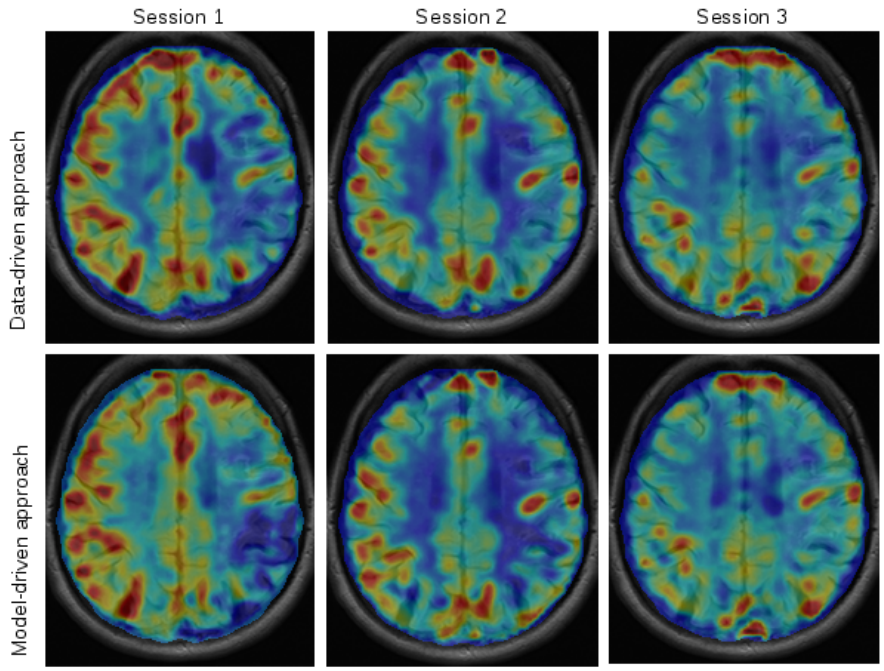

Figure 6.13. CVR improvement for a single patient after stent treatment is shown in three session. The patient had a extracranial stenosis of the left ICA. The CVR impairement is clearly visible for both methods. On the second session, some CVR impaitement is still visible, though the DDA method is less sensitive in detecting it. On the third session, the CVR impairement is no more visible in the CVR maps of both methods.

6.5 Methods evaluation – summary

With the data-driven method, the overall quality of CVR maps improved in 12 cases out of 31 (39%) and in 32 out of 42 (76%), in the evaluation by the board of physicians and by the medical physicist, respectively. In the board evaluation, there was 17% (10 out of 58) unreadable cases in the model-driven method evaluation, and 10% (3 out of 31) in the data-driven method. In the physicist evaluation, there was 12% unreadable in the model-driven method and 3% in data-driven method. In the 'Improved findings' case, the data-driven was correct in 55% (66%[1]) (6 out of 11) cases in the board evaluation and 66% (16 out of 24) (84%[2]) cases in the physicist evaluation.

Score	Board		Physicist	
	MDA	DDA	MDA	DDA
Quality improvement	13%	39%	5%	76%
Unreadable cases	17%	10%	12%	3%
Diagnose correct	45% (34%)	55% (66%)	34% (16%)	66% (84%)
Final score	5 (3) pts	13 pts	9 (4) pts	33 pts

Table 6.3. Summary of the results. Quality improvement – in how many cases the quality improved between methods; Unreadable cases – how many sessions scored 0; Improved findings – how many cases were correct for the particular method. Final score – from tables 6.1 and 6.2 (pts – points; MDA – model-driven approach; DDA – data-driven approach).

[1]) not considering the case of 3 sessions that were evaluated differently while the images were identical
[2]) not considering the 5 cases of lesser sensitivity of data-driven in the follow-ups after treatment

Chapter 7
Discussion

In this work, we have reached all the main goals set in the thesis proposal. The data were successfully acquired and processed and the output were CVR maps that could be directly used in evaluation of CVR impairment. Moreover, we have designed and implemented a novel method for data-driven processing of hypercapnia BOLD data, that was shown to give more reliable results than the standard method of evaluation. We have, however, faced several challenges during the implementation and evaluation which are discussed in this section. We also give directions in which the future development of our method can go to obtain even better results.

7.1 Delay

For analyzing the response delay, two methods were used. The first was a subject-wise correction (SWC) which shifts the regressor in time to the point of largest correlation with mean patient response. We have also tried a pixel-wise correction (PWC) method which shift data in each voxel in time to the point of largest correlation with the regressor. The PWC method aimed to compensate for region-wise delays as demonstrated by Blockley (the time-difference in response in temporal and frontal areas was shown to be up to couple of seconds [35]). We have, however, observed that the CVR-maps generated using the pixel-wise correlation method had reduced sensitivity to detecting impaired regions. This is supported by the findings of Bhogal that the impaired response of CVR have different temporal characteristics than the healthy one [52]. For this reason, we have used only the subject-wise delay correction in the final evaluation. A solution to this problem might be to use a designated regional delays based on mean regional delays calculated in healthy subjects.

7.2 Regressors

Apart from the model-driven and data-driven methods described in previous section, several other regressors were implemented (e.g. HRF with time derivative [46], a respiratory-response function (RRF) [78]). However, no significant changes of quality were observed, thus these methods were not included in the comparison.

It is interesting to note the difference between end–inspiration and end–expiration methods of breath holding. The end–expiration is used more frequently though it is less comfortable for the subjects. The reason is that the increase of CO_2 is faster and thus the response has shorter delay than in end–inspiration. The response has similar shape as the haemodynamic response function (figure 7.1) and thus is more easily modelled by classical approach of convolving box function with HRF curve. On the other hand, breath holding after inspiration takes less effort for the examined subjects. This was the reason why we chose it for our study. However, the BOLD response contains one

additional smaller peak. This probably occurs because of sudden oxygen saturation, see Figure 7.2. This complicates the analysis, as this smaller peak is often present also in pathological regions that otherwise have a paradoxical response in hypercapnia-BOLD. We have developed an advanced data-driven method that tries to remove the smaller peak from the data-driven method regressor to reduce the effect of this on the CVR analysis (method RP in the processing pipeline). Although we have failed to improve the results significantly, we strongly believe, that looking at the response during inspiration and during breath-holding separately can bring additional important information in the hypercapnia-BOLD evaluation.

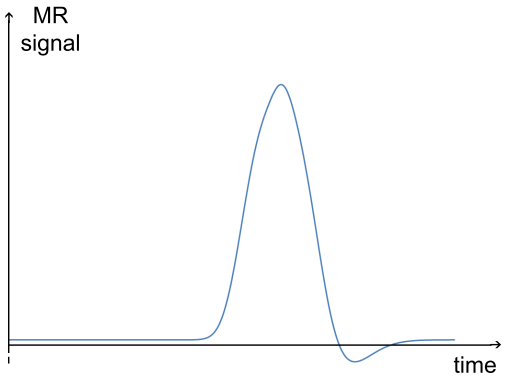

Figure 7.1. Shape of response to breath hold after expiration.

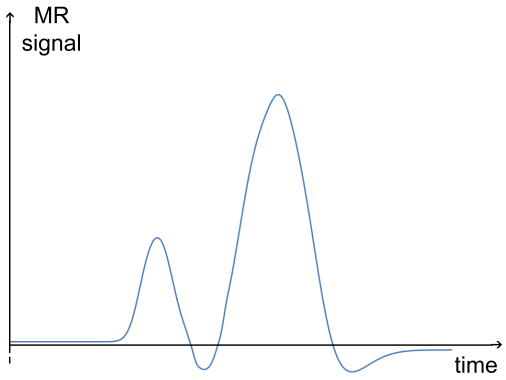

Figure 7.2. Shape of response to breath hold after inspiration.

The ideal option to verify the performance of model-driven and data-driven methods would be to test the methods on healthy volunteers and introduce artificial errors in the breath-holding protocol (missed breath-holds, errors in timing etc.) while measuring also the concentration of exhaled CO_2 using a capnometer as this gives an almost ideal regressor for CVR evaluation.

We have also tested an iterative method for data analysis. In the first iteration, the model driven approach was used. The voxels showing significant positive activation were assumed to belong to healthy tissue. Their time response was averaged and used as a regressor in the following iteration. This was repeated until convergence (the difference between the sets of activated voxels between iterations was less than 10 voxels). We have, however, not observed any major changes in the results of the DDA and iterative method.

7.3 Evaluation

Both evaluations gave a clear result that the proposed method (DDA) can offer at least the same quality of the results as the MDA method in the fully-cooperating subjects. Moreover, it can significantly improve the quality in the case of a subject that deviates from the breathing protocol. There are, however, several shortcomings of the evaluation procedure performed.

While the TOF and FLAIR can in most cases confirm the findings from hypercapnia BOLD, it cannot be taken as ground-truth for the CVR-impairment evaluation. Presence of infarct should imply also CVR impairment, however, it does not necessarily

work the other way around. The impaired CVR most probably imply stenosis, however, the stenosis does not necessarily cause decrease in CVR. A reliable ground-truth can be obtained by measuring the concentration of the exhaled CO_2 as well for reference which we plan to in the future.

In 72% cases(153 sessions), the resulting quality was 2 for both DDA and MDA. In 47% cases(58 sessions), the quality was 2 on MDA and thus it was not assessed for DDA. However, the main point of interest are the cases 'Improved findings', 'Same findings' and 'Undecided' which contributed the most for the comparison of the efficiency of the two methods. There, a the DDA method performed better in the majority of cases. Only in few cases, it was not possible to decide what findings from which method are more reasonable.

In the evaluation by the board of physicians, three patients were evaluated as having a better diagnostic quality in the MDA images (DDA quality score 0, MDA quality score 1). While reviewing the results, we have noted that the DDA and MDA maps were identical identical. This can be thus attributed to the error of the raters. Careful reviewing of other cases have not revealed any other similar error.

In the medical-physicist evaluation, the quality evaluation the diagnostic potential was done first. Then, the findings from multiple sessions in one patient (if available) were compared to find pathological regions that were visible throughout all sessions and thus be able to decide about correctness of findings in individual sessions if the quality of the map was questionable. The later session were usually measured after treatment the CVR improved in most of the subject. In 5 cases in one of later sessions, MDA proved higher sensitivity in detecting pathological regions than the DDA method. While still some small regions with impaired CVR were visible on the MDA-maps, they were smaller or even appeared completely normal in the DDA method. However, this kind of findings was visible only in the follow-up sessions and would thus not have a great impact on the diagnostics.

In total, 3 cases in physician evaluation and 5 cases in physicist evaluation had score 0 for both methods. The reason in all cases was identified as too low SNR in the mean response (no detectable pattern of normal breathing and breath-holds was visible). The possible reason is that these patients did not held breath for sufficiently long time or completely skipped several BH periods. Interestingly, the physicist and physicians independently marked only 1 session as unreadable for both methods. Three cases were not evaluated by the board of physicians, two and one cases were marked as readable by at least one of the methods by the physicist and the physicians, respectively.

An further experimental validation of method is planed to be done on healthy subjects. A similar measurement to the current one will be done while measuring also the concentration of CO_2 in exhaled gas. This would allow a more rigorous comparison of the MDA and DDA methods as the CVR-maps obtained using the CO_2 curve as a regressor are close to the ground-truth. Poor performance of the subjects will be simulated by intentionally not doing all BH tasks, by delayed response to commands, by ending the BH prematurely or by hyperventilating between BH periods.

Chapter 8
Conclusion

All the goals from the thesis specification were accomplished as further specified by the following list:

- Learn the principles of functional MR imaging and data processing
  - The basics of MRI and fMRI are briefly described in Chapter 2.
  - The theory and already published methods for assessing CVR with hypercapnia are described in Chapter 3
- Design and implement a method for evaluation of hypercapnia sequences, to distinguish between normal and pathological regions.
  - A pipeline for automatic processing of hypercapnia BOLD data was implemented. The inputs are BOLD EPI and FLAIR images in DICOM format and the output is a CVR-map overlayed over a FLAIR image normalized to the MNI template (Section 5.2).
  - A standard evaluation of the vascular response assuming the block design experiment was implemented. The individual delays in the patients response to commands were corrected for (Section 5.2.2).
  - A novel data-driven approach which robustly evaluates the data even when the subject is not following the measurement protocol precisely was implemented (Section 5.2.2).
- Experimentally evaluate the developed method on provided clinical data.
  - The CVR-maps were calculated on a group of patients to provide an additional information for a clinical study of patients with cerebrovascular pathology (Section 5.3).
  - The quality of the CVR-maps for the standard and novel analysis were compared. The pathological findings of the two methods were also compared (Sections 6.3 and 6.4) and a clear improvement of the proposed method was shown.

The proposed data-driven approach is a promising tool to assess CVR in clinical population. It gives reasonable results in case the standard analysis completely fails given that the patient did not deviate too much from the breathing protocol and he held breath for sufficiently long time. The quality of the CVR-maps improved in 39% cases (out of 31 session which scored 0 or 1 on MDA; physicians) and 76% cases (out of 42 session which scored 0 or 1 on MDA; physicist) using the new method and in 66% it also improved the pathological findings.

However, the data-driven approach also fails in the situations when the subject did not hold breath for sufficient time to generate an adequate response or did deviate from the protocol in any other way. Further investigation has to be carried out to assess the diagnostic benefit of using this method and to do a more thorough analysis on a larger number of subjects.

Analysis on a healthy volunteers comparing the MDA, DDA and a method using a $P_{ET}CO_2$ curve as a regressor is planned to have a ground-truth observation and to be able to more thoroughly compare the methods in the presence of various complications in the acquisition process. It is not expected that the data-driven approach would exceed the quality of the results that uses the $P_{ET}CO_2$ curve as a regressor, however, the proposed method nevertheless brings a very important improvement in the hypercapnia-BOLD analysis. Its main strength is that this method can be easily implemented in the processing pipeline of any clinical station. Whereas the $P_{ET}CO_2$ measurement is a complicated process and the hardware is not commonly available and very much complicates the hypercapnia-BOLD to be widely used.

Chapter 9
Appendix

9.1 The Bloch equations

The Bloch equations describe what is detected in the receiver coil of an MRI scanner. Matrix-vector notation:

$$\frac{d}{dt}\begin{pmatrix} M_x \\ M_y \\ M_z \end{pmatrix} = \begin{pmatrix} -\frac{1}{T2} & \gamma B_z & -\gamma B_y \\ -\gamma B_z & -\frac{1}{T2} & \gamma B_x \\ \gamma B_y & -\gamma B_x & -\frac{1}{T1} \end{pmatrix} \cdot \begin{pmatrix} M_x \\ M_y \\ M_z \end{pmatrix} + \begin{pmatrix} 0 \\ 0 \\ \frac{M_0}{T1} \end{pmatrix}, \tag{9.1}$$

nuclear magnetization $\mathbf{M} = (M_x, M_y, M_z)$ in external magnetic field $\mathbf{B} = \mathbf{B_0} + \mathbf{B_1}$ experienced by nuclei, z component of $\mathbf{B}$ is composed of two terms B_0 is main magnetic field, constant in time and $\mathbf{B_1}$ may be time dependent and helps with spatial decoding of the NMR signal. γ is a gyromagnetic ratio. M_0 is the steady state magnetization.

9.2 Masks and slice selection

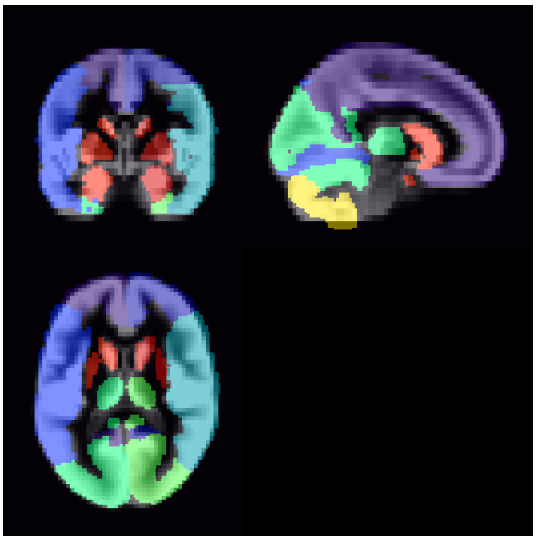

Figure 9.1. 10 ROI mask: 1,2 – ACA; 3,4 – MCA; 5,6 – PCA; 7,8 – BA, 9,10 ACHA; designed by the supervising physician.

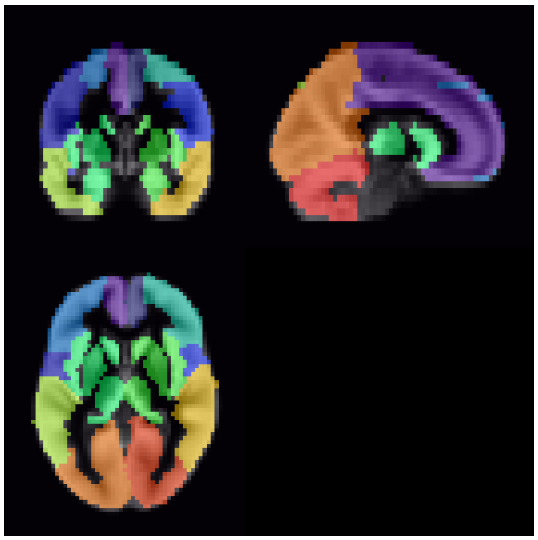

Figure 9.2. 15 ROI mask:1,2 – ACA; 3,4 – MCAA; 5,6 MCAM; 7,8 – central; 9,10 – MCAP; 11,12 – PCA; 13,14 – vert, 15 – vermis; designed by author in need for detailed region map with approximately same size.

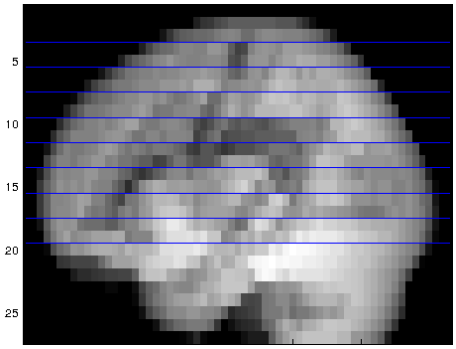

Figure 9.3. Slices 9

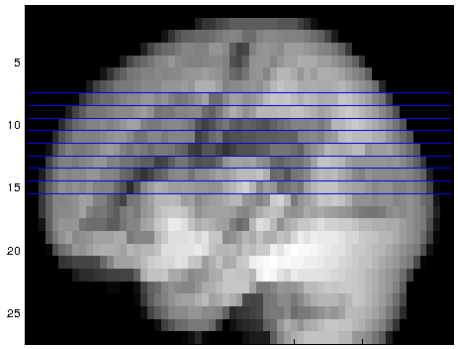

Figure 9.4. Slices 9 version b

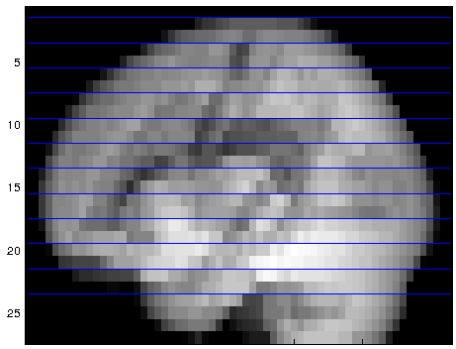

Figure 9.5. Slices 12

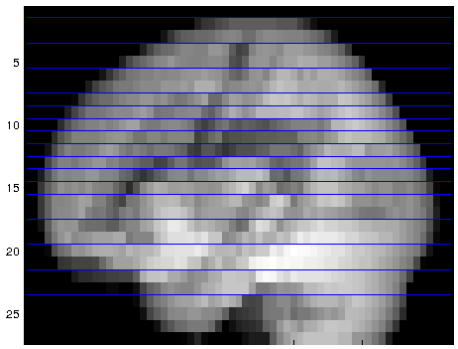

Figure 9.6. Slices 16

9.3 Codes

In this section, we describe the functionality of the most important scripts in Matlab. We also describe the outputs and inputs of the analysis software and we provide a simple manual on adding and analyzing a new subject with the methods. Matlab, SPM and dcm2nii have to be installed.

For proper function of all scripts, the analyzed data have to be in following folder structure:

```
data
- CVR_000
- - Session_00
- - - dicom
- - - CVR_000_Session_00_SHIFT_METHOD_MASK
- - - original_CVR_000_Session_00.nii
- - - roriginal_CVR_000_Session_00.nii
- - - s6wroriginal_CVR_000_Session_00.nii
- - - meanoriginal_CVR_000_Session_00.nii
- FLAIR
- - dicom
- - - CVR_000_FLAIR.nii
```

Preprocessing: Only input necessary to specify in the `preprocess_launcher.m` is the path to the file. Preprocessing generates multiple files in the `../Session_00` folder, however the important one is with prefix `s6wr`.

Processing: The setting is done via script `modelDesign.m` which allows multiple parameters to be changed:

```
%% basic settings
% model
resultfolder='results/' %lsqf results folder
curv={ 'hrf', 'hrf2', 'rrf', 'rrf2', 'mean'}; %initial regressor
shif={'SWC','PWC'}; %shift method
shiftRange=[0, 2, 3 ];% maximal shift range
bestfit={'off','on', 'BP', 'RP'}; % bestfit setting/peak removeal
ROImask=[7, 10, 15]; % region mask, default 7 regions
scalp=[1,0]; % scalp as one of the regions
dt=[1 0]; % include time derivation of regressor in analysis
iter=[1 2 3]; % iteration
P='spmRes0001'; %iteration calculated in pixels activated at
  % 'spmRes05', 'spmRes01','spmRes001'

%% parameters for extraction SPM8 analysis
thresDesc='FWE'; % - 'FWE' or 'none' - family wise error correction
thresholdCluster= 10; % - minimal size of activated cluster
c=[1 -1; 0 0]; % -contrast
th=0.0001; % treshold
```

Visualization: Is run trough `plots.m`. Only the input and output folders, and number of slices in the visualization needs to be specified.

9.4 Analyze new subject

Here is a simple cookbook on how to analyze a new subject:

1. Download DICOM files using dicom2ecat program to a new patient folder (note that this program is specific for our site and a different interface to access the PACS system has to be used on different site):

   a) `../data/CVR_xyz/Session_cd/dicom` (for EPI),
   b) `../data/CVR_xyz/FLAIR/dicom` (for FLAIR)

2. Transform DICOM files to NIFTI using a script: `/preprocessing/dicom2nifti.m` (variant for EPI, FLAIR/Single, Multiple). Names of all directories to be processed needs to be specified on `names.txt`.
3. Do the preprocessing:

   a) for EPI - use the preprocessing routine using `preprocess_launcher.m`,
   b) for FLAIR only spatial normalization is needed. This is done using SPM: Normalise: Estimate and Write with voxel size [0.3,0.3,6.5] - necessary for future coregistration! If no anatomical image is available, mean of EPI can be used instead. The mean EPI file is created during preprocessing routine - copy it to the FLAIR folder, do the registration as specified above and rename the result to 'CVR_xyz_FLAIR.nii'.

4. Processing: script named `modelDesign.m` allows multiple settings. Mandatory input is the list of directories to be processing `names.txt`. The script saves multiple files according to settings described above. To save CVR maps for several slices in png coregistered to anatomical image, use a script named `plots.m`.

9.5 Folder system

Here is a list of all matlab file with a brief description of the function of each of it. The files are organized into directories according to the function. The following notation is used: (s) for script, (f) for function.

```
codes
| - preprocessing
| | - dicom2nifti.m"(s): runs dcm2nii program with pre-set parameters
| | - walker.m"(f): used by "dicom2nifti.m" when run on folder tree
| | - preprocess_launcher.m(s): runs SPM8 preprocessing
| | - realign.m(f): realign parameter file
| | - normestm.m(f): normalize - estimate paramter file
| | - normwrite.m(f): normalize - write parameter file
| | - smoothing.m(f): smoothing parameter file
| | - foldercheck.m(f): supporting function checks file content
| - motion
| | - motion.m(s): extract movement info from files generated by realign
| | - motionstat.m(s): calculates movement statistics
| | - statplot.m(s): visualisation tool
| - processing
| | - modelDesign.m(s): setting up all parameters for data analysis
| | - names.txt: contains the names of sessions to be analyzed
| | - makeModel.m(f): runs all the processing according to modelDesign
| | - curves.mat: file containing the initial regressors
| | - getmean.m(f): mean curve calculation
| | - meanOverROI.m(f): mean curves in ROI calculation
| | - removeDrift.m(f): highpass filter
| | - filtration.m(f): lowpass filter
| | - crosscorrreduced.m(f): subject-wise lag calculation and shift
| | - pixelWiseCrosscorr.m(f): pixel-wise lag calculation
| | - shiftpix.m(f): pixel wise shift
| | - getBestROI.m(f): sets the ROI with the best PCC as regressor
| | - corrcoef.m(f): pearsons correlation coeficient calculation
| | - lsqfitting.m(f): generate CVR-map as *.nii
| | - lsqf.m"(f): calculates least square fitting
| | - spm_analysis.m(f): setting paramters for spm8 data analysis
| | - saveimg.m(f): saves semi results and results
| - temp_reg
| | - BasicLabels.nii: 7 ROI mask
| | - MediumLabels.nii: 10 ROI mask
| | - DetailedLabels.nii: 15 ROI mask
| | - TMP.nii: 6 masks for GM, WM, CSF, scalp, bone and head
| | - skalp.nii: scalp mask
| - results_extr
| | - resut_extract.m(f): extracts results from SPM data analysis
| | - fMRIContrasf(f): search for active voxels
| | - spm_...(f): modified spm functions for manipulating NIFTI files
| - plot
| | - plots.m(s): runs function plotresult.m on selected files
| | - plotresult.m(f): creates FLAIR CVR-map overlay and saves
```

9.6 List of abbreviations

- ACA — Anterior Cerebral Artery
- AD — Alzheimer's Disease
- ASL — Arterial Spin Labelling
- ATP — Adenosine Triphosphate
- AVM — ArterioVenous Malformation
- BA — Basilar Artery
- BOLD — Blood Oxygen Level Dependent
- CBF — Cerebral Blood Flow
- $CMRO_2$ — Cerebral Metabolic Rate for Oxygen
- CTA — Computed Tomography Angiography
- CVR — Cerebral Vessel Reactivity
- DIND — Delayed Ischemic Neurological Deficit
- DSA — Digital Subtraction Angiography
- FLAIR — Fluid Attenuated Inversion Recovery
- fMRI — functional Magnetic Resonance Imaging
- GLM — Generalized Linear Model
- HR — Haemodynamic Response function
- HRF — Haemodynamic Response Function
- ICA — Internal Carotid Artery
- LSQF — Leas SQuares Fitting
- MCA — Middle Cerebral Artery
- MCI — Mild Cognitive Impairment
- MRA — Magnetic Resonance Angiography
- MRI — Magnetic Resonance Imaging
- NVC — Neurovascular Coupling
- P_aCO_2 — Arterial Partial Pressure of CO_2
- $P_{ET}CO_2$ — End Tidal Partial Pressure of CO_2
- PCA — Posterior Cerebral Artery
- PCC — Pearsons Correlation Coefficient
- PET — Positron Emission Tomography
- PWC — Pixel-Wise Correction
- ROI — Region Of Interest

SNR	Signal to Noise Ratio
SPECT	Single Proton Emission Tomography
SWC	Subject-Wise Correction
TCD	Transcranial Doppler Ultrasonography
TE	Echo Time
TOF	Time Of Flight angiography
TR	Repetition Time
VA	Vertebral Artery

References

[1] Dumville, J., R. B. Panerai, N.S. Lennard, A. R. Naylor, and D.H. Evans. Can cerebrovascular reactivity be assessed without measuring blood pressure in patients with carotid artery disease?. *Stroke a journal of cerebral circulation* . 1998, Vol. 29, No. 5, pp. 968-974.

[2] Wise, Richard G., Kojiro Ide, Marc J. Poulin, and Irene Tracey. Resting fluctuations in arterial carbon dioxide induce significant low frequency variations in BOLD signal. *Neuroimage*. 2004, Vol. 21, pp. 1652-1664.

[3] Pillai, Jay J., and David J. Mikulis. Cerebrovascular Reactivity Mapping: An Evolving Standard for Clinical Functional Imaging. *American Journal of Neuroradiology*. 2014, Vol. 00, pp. 00-00.

[4] *Questions and Answers in NMR*. `http://mri-q.com/who-discovered-nmr.html`.

[5] McRobbie, Donald W., and et al. *MRI from Picture to Proton*. Cambridge University Press, 2007. ISBN 0-521-52319-2 .

[6] Bernstein, Matt A., Kevin F. King, and Xiaohong Joe Zhou. *Handbook of MRI pulse sequences*. Academic Press, 2004. ISBN 978-0-12-092861-3 .

[7] *The Nobel Prize in Physiology or Medicine for 2003 - Press Release*. `http://www.nobelprize.org/nobel_prizes/medicine/laureates/2003/press.html`.

[8] Bélanger, "Mireille, Igor Allaman, and Pierre J. Magistretti". "Brain Energy Metabolism: Focus on Astrocyte-Neuron Metabolic Cooperation ". *"Cell Metabolism "*. "2011", Vol. "14", No. "6", pp. "724 - 738".

[9] Wang, Yonker, and Shi-Jiang Li. *Differentiation of metabolic concentrations between gray matter and white matter of human brain by in vivo1H magnetic resonance spectroscopy*.

[10] Pasley, Brian N., and Ralph D. Freeman. Neurovascular Coupling. *Scholarpedia*. 2008, Vol. 3, No. 3, pp. 5340. `http://www.scholarpedia.org/article/Neurovascular_coupling`.

[11] Rengachary, Setti S, and Richard G Ellenbogen. *Principles of neurosurgery*. Elsevier Mosby, 2005.

[12] Schwertfeger, N., P.Schlattmann, H. Lemke, I. Heuser, and M. Bajbouj. Cerebrovascular Reactivity Over Time Course in Healthy Subjects. *Journal of Neurological Sciences*. 2006, Vol. 249, pp. 135-139.

[13] Hill, Lisa. *Cerebral Blood Flow and Intracranial Pressure pt.1*. `http://www.frca.co.uk/Documents/170907%20Cerebral%20physiology%20I.pdf`.

[14] Hill, Lisa. *Cerebral Blood Flow and Intracranial Pressure pt.2*. `http://www.frca.co.uk/Documents/011007Cerebral%20Physiology%20II.pdf`.

[15] Kim, Seong-Gi, and Seiji Ogawa. Biophysical and physiological origins of blood oxygenation level-dependent fMRI signals. *Cereb Blood Flow Metab*. 2012, Vol. 32, No. 7, pp. 1188-1206.

[16] Kassner, Andrea, Jeff D. Winter, Julien Poublanc, David J. Mikulis, and Adrian P. Crawley. Blood-Oxygen Level Dependent MRI Measures of Cerebrovascular Reactivity Using a Controlled Respiratory Challenge: Reproducibility and Gender Differences. *Journal of MRI*. 2010, Vol. 31, pp. 298-304.

[17] Sobczyk, O., A. Battisti-Charbonney, J. Fierstra, D.M. Mandell, J. Poublanc, P. Crawley, D. J. Mikulis, J. Duffin, and J. Fisher. A conceptual model for CO_2-induced redistribution of cerebral blood flow with experimental confirmation using BOLD MRI.. *NeuroImage*. 2014, Vol. 92, pp. 56–68.

[18] Abdulrauf, Saleem I.. *Cerebral Revascularization: Techniques in Extracranial-to-Intracranial Bypass Surgery: Expert Consult*. Elsevier Health Sciences, 2010.

[19] Hare, Hannah V., Michael Germuska, Michael E. Kelly, and Daniel P. Bulte. Comparison of CO2 in air versus carbogen for the measuremnt of cerebrovascular reactivity with magnetic resonance imaging. *Journal od Cerebral Blood Flow and Metabolism*. 2013, Vol. 33, pp. 1799-1805.

[20] Pauling, Linus, and Charles Coryell. The Magnetic Properties and Structure of Hemoglobin Oxyhemoglobin and Carbonmonoxyhemoglobin. *Proc Natl Acad Sci U S A*. 1936, Vol. 22, No. 4, pp. 210-216.

[21] Ogawa, S., T. M. Lee, A. R. Kay, and D. W. Tank. Brain magnetic resonance imaging with contrast dependent on blood oxygenation. *Biophysics*. 1990 , Vol. 87, pp. 9868-9872.

[22] Carr, J.C., and T.J. Carroll. *Magnetic Resonance Angiography: Principles and Applications*. Springer, 2011. ISBN 978-1-44-191686-0.

[23] Posse, Stefan, Lars J. Kemna, Barbara Elghahwagi, Stefan Wiese, and Valerij G. Kiselev. Effect of graded hypo and hypercapnia on fMRI contrast in visual cortex: Quantification of T2* changes by multiecho EPI. *Magnetic Resonance in Medicine*. 2001, Vol. 46, No. 2, pp. 264-271.

[24] Logothetis, Nikos K.. What we can do and what we cannot do with fMRI. *Nature*. 2008, No. 7197, pp. 869-878.

[25] Frahm, Jens, and Klaus Merboldt. Brain or vein-oxygenation or flow? On signal physiology in functional MRI of human brain activation. *NMR in Biomedicine*. Vol. 7, No. 1-2, pp. 45 - 53 year = 1994. ISSN 1099-1492.

[26] Chlebus, P., M. Mikl, M. Brázdil, and P. Krupa. Funkční magnetická rezonance-úvod do problematiky. *Neurologie pro praxi*. 2005, No. 3, pp. 133-138 .

[27] Liau, Joy, and Thomas T. Liu. Inter-subject variability in hypercapnic normalization of the BOLD fMRI response . *NeuroImage* . 2009, Vol. 45, No. 2, pp. 420-430.

[28] Thomason, Moriah E., Lara C. Foland, and Gary H. Glover. Calibration of BOLD fMRI using breath holding reduces group variance during a cognitive task. *Human Brain Mapping*. 2007 , Vol. 28, No. 1, pp. 59-68.

[29] Thomason, Moriah E., Brittany E. Burrows, John D.E. Gabrieli, and Gary H. Glover. Breath holding reveals differences in fMRI BOLD signal in children and adults . *NeuroImage* . 2005, Vol. 25, No. 3, pp. 824-837.

[30] Cohen, Eric R., Egill Rostrup, Karam Sidaros, Torben E. Lund, Olaf B. Paulson, Kamil Ugurbil, and Seong-Gi Kim. Hypercapnic normalization of BOLD fMRI: comparison across field strengths and pulse sequences . *NeuroImage* . 2004, Vol. 23, No. 2, pp. 613-624.

[31] Buxton, Richard B. Coupling between CBF and $CMRO_2$ during neuronal activity . *International Congress Series* . 2002, Vol. 1235, No. 0, pp. 23-32.

[32] Buxton, Richard B.. The physics of functional magnetic resonance imaging (fMRI). *Reports on Progress in Physics*. 2013 , Vol. 76, pp. 30.

[33] Pillai, Jay J., and Domenico Zaca. Clinical utility of cerebrovascular reactivity mapping in patients with low grade gliomas. *WJCO*. 2011, Vol. 2, No. 12, pp. 397-403.

[34] Shen, Yuji, Trevor Ahearn, Matthew Clemence, and Christian Schwarzbauer. Magnetic resonance imaging of the mean venous vessel size in the human brain using transient hyperoxia. *NeuroImage*. 2011 , Vol. 55, No. 3, pp. 1063-1067.

[35] Blockley, Nicholas P., Valerie E.M. Griffeth, Aaron B. Simon, and Richard B. Buxton. A review of calibrated blood oxygenation level dependent (BOLD) methods for the measurement of task induced changes in brain oxygen metabolism. *NMR in Biomedicine*. 2013 , Vol. 26, No. 8, pp. 987-1003.

[36] Chiarelli, Peter A., Daniel P. Bulte, Richard Wise, Daniel Gallichan, and Peter Jezzard. A calibration method for quantitative BOLD fMRI based on hyperoxia. *Neuroimage*. 2007, Vol. 37, pp. 808-820.

[37] Duong, Timothy Q., Costantino Iadecola, and Seong-Gi Kim. Effect of hyperoxia hypercapnia and hypoxia on cerebral interstitial oxygen tension and cerebral blood flow. *Magnetic Resonance in Medicine*. 2001, Vol. 45, No. 1, pp. 61-70.

[38] Jain, V., C. Langham, and et al. Rapid magnetic resonance measurement of global cerebral metabolic rate of oxygen consumption in humans during rest and hypercapnia. *Cereb Blood Flow Metab*. 2011, Vol. 31, No. 7, pp. 1504-1512.

[39] Kastrup, Andreas, Gunnan Krüger, Tobias Neumann-Haefelin, and Michael E. Moseley. Assesment of cerebrovascular reactivity with functional magnetic resonance imaging: comparison of CO2 and breath holding. *Magnetic resonance imaging*. 2001, Vol. 19, pp. 13-20.

[40] Bright, Molly G., Daniel P. Bulte, Peter Jezzard, and Jeff H. Duyn. Characterization of regional heterogeneity in cerebrovascular reactivity dynamics using novel hypocapnia task and BOLD fMRI . *NeuroImage* . 2009 , Vol. 48, No. 1, pp. 166-175.

[41] Goode, S.D., S. Krishan, C. Alexakis, R. Mahajan, and D.P. Auer. Precision of Cerebrovascular Reactivity Assessment with Use of Different Quantification Methods for Hypercapnia Functional MR Imaging. *American Journal of Neuroradiology* . 2009, Vol. 30, No. 5, pp. 972-977.

[42] Cantin, S., M. Villien, O. Moreaud, I. Tropres, S. Keignart, E. Chipon, J.-F. Le Bas, J. Warnking, and A. Krainik. Impaired cerebral vasoreactivity to CO2 in Alzheimer's disease using BOLD fMRI . *NeuroImage* . 2011, Vol. 58, No. 2, pp. 579-587.

[43] Stefanovic, Bojana, Jan M. Warnking, Karin M. Rylander, and G. Bruce Pike. The effect of global cerebral vasodilation on focal activation hemodynamics . *NeuroImage* . 2006, Vol. 30, No. 3, pp. 726-734.

[44] Xu, Feng, and et al. The influence of carbon dioxide on brain activity and metabolism in conscious humans. *Cereb Blood Flow Metab*. 2011, Vol. 31, No. 1, pp. 58-67.

[45] Yezhuvath, Uma S., Kelly Lewis-Amezcua, Rani Varghese, Guanghua Xiao, and Hanzhang Lu. On the assessment of cerebrovascular reactivity using hypercapnia BOLD MRI. *NMR in Biomedicine*. Vol. 22, No. 7, pp. 779-786 .

[46] Murphy, Kevin, Ashley D. Harris, and Richard G. Wise. Robustly measuring vascular reactivity differences with breath-hold: Normalising stimulus-evoked and resting state BOLD fMRI data. *Neuroimage*. 2011, Vol. 54, pp. 369-379.

[47] Kastrup, Andreas, Tie-Qiang Li, Atsuchi Takahashi, Gary H. Glover, and Michael E. Moseley. Functional Magnetic Resonance Imaging of Regional Cerebral Blood Oxygenation Changes During Breath Holding. *Stroke* . 1998, Vol. 29, No. 12, pp. 2641-2645.

[48] Kastrup, Andreas, Gunnar Krüger, Gary H. Glover, and Michael E. Moseley. Assessment of cerebral oxidative metabolism with breath holding and fMRI. *Magnetic Resonance in Medicine*. 1999 , Vol. 42, No. 3, pp. 608-611.

[49] Kastrup, Andreas, Gunnar Krüger, Gary H. Glover, Tobias Neumann-Haefelin, and Michael E. Moseley. Regional Variability of Cerebral Blood Oxygenation Response to Hypercapnia . *NeuroImage* . 1999, Vol. 10, No. 6, pp. 675-681.

[50] Spano, V. R., D. M. Mandell, and J. Poublanc. CO2 Blood Oxygen Level – dependent MR Mapping of Cerebrovascular Reserve in a Clinical Population: Safety, Tolerability, and Technical Feasibility. *Radiology*. Vol. 266, pp. 592-598.

[51] Fierstra, Jorn, John Conklin, Timo Krings, Marat Slessarev, Jay S. Han, Joseph Fisher, Karel Terbrugge, M. Christopher Wallace, Michael Tymianski, and David J. Mikulis. Impaired peri-nidal cerebrovascular reserve in seizure patients with brain arteriovenous malformations. *Brain*. 2011, Vol. 134, No. 2010, pp. 100–109.

[52] Bhogal, Alex, Jeroen C. W. Siero, Joseph Fisher, Martijn Froeling, Peter Luijten, Marielle Philippens, and Hans Hoogduin. Investigating the non-linearity of the BOLD cerebrovascular reactivity response to targeted hypo/hypercapnia at 7T. *NeuroImage*. Elsevier Inc., 2014, Vol. 98, pp. 296–305.

[53] Symon, L.. Experimental Evidence for "Intracerebral Steal" following CO2 Inhalation. *Scandinavian Journal of Clinical and Laboratory Investigation*. 1968, Vol. 21, No. s102, pp. XIII-A-XIII-A.

[54] Brawley, B. W.. The Pathophysiology of Intracerebral Steal following Carbon Dioxide Inhalation, an Experimental Study. *Scandinavian Journal of Clinical and Laboratory Investigation*. 1968, Vol. 21, No. s102, pp. XIII-B-XIII-B.

[55] Harper, A M, and H I Glass. Effect of alterations in the arterial carbon dioxide tension on the blood flow through the cerebral cortex at normal and low arterial blood pressures.. *Journal of Neurology, Neurosurgery and Psychiatry*. 1965, Vol. 28, No. 5, pp. 449-452.

[56] Faraci, Frank M, and Donald D Heistad. Regulation of large cerebral arteries and cerebral microvascular pressure.. *Circulation research*. Am Heart Assoc, 1990, Vol. 66, No. 1, pp. 8–17.

[57] Fierstra, Jorn, David B. MacLean, Joseph Fisher, Jay S. Han, Daniel M. Mandell, John Conklin, Julien Poublanc, Adrian P. Crawley, Luca Regli, David J. Mikulis, and Michael Tymianski. Surgical revascularization reverses cerebral cortical thinning in patients with severe cerebrovascular steno-occlusive disease. *Stroke*. 2011, Vol. 42, pp. 1631–1637.

[58] Mandell, D.M., J.S. Han, J. Poublanc, A.P. Crawley, J. Fierstra, M. Tymianski, J.A. Fisher, and D.J. Mikulis. Quantitative Measurement of Cerebrovascular

Reactivity by Blood Oxygen Level-Dependent MR Imaging in Patients with Intracranial Stenosis:Preoperative Cerebrovascular Reactivity Predicts the Effect of Extracranial-Intracranial Bypass Surgery. *American Journal of Neuroradiology* . 2011, Vol. 32, No. 4, pp. 721-727.

[59] Conklin, John, Jorn Fierstra, Adrian P. Crawley, Jay S. Han, Julien Poublanc, Daniel M. Mandell, Frank L. Silver, Michael Tymianski, Joseph A. Fisher, and David J. Mikulis. Impaired Cerebrovascular Reactivity With Steal Phenomenon Is Associated With Increased Diffusion in White Matter of Patients With Moyamoya Disease. *Stroke* . 2010, Vol. 41, No. 8, pp. 1610-1616.

[60] Costa, Leodante da, Jorn Fierstra, Joseph A. Fisher, David J. Mikulis, Jay S. Han, and Michael Tymianski. BOLD MRI and Early Impairment of Cerebrovascular Reserve After Aneurysmal Subarachnoid Hemorrhage. *Journal of MRI*. 2013, Vol. 00, pp. 00-00.

[61] Chang, Ting Yu, Wan Chun Kuan, Kuo Lun Huang, Chien Hung Chang, Yeu Jhy Chang, Ho Fai Wong, Tsong Hai Lee, and Ho Ling Liu. Heterogeneous Cerebral Vasoreactivity Dynamics in Patients with Carotid Stenosis. *PLoS ONE*. 2013, Vol. 8, No. 9, pp. 1–10.

[62] Poublanc, Julien, Jay Show Han, Daniel Michael Mandell, John Conklin, Jeffrey Alan Stainsby, Joseph Arnold Fisher, David John Mikulis, and Adrian Philip Crawley. Vascular steal explains early paradoxical blood oxygen level-dependent cerebrovascular response in brain regions with delayed arterial transit times.. *Cerebrovascular diseases extra*. 2013, Vol. 3, pp. 55–64.

[63] Jochimsen, Thies H., Harald E. Möller, Dimo Ivanov Jürgen R. Reichenbach, Derek V.M. Ott, Wolfgang Heinke, and Robert Turner. Whole-brain mapping of venous vessel size in humans using the hypercapnia-induced BOLD effect. . *NeuroImage*. 2010 , Vol. 51, No. 2, pp. 765-774.

[64] Heyn, C., J. Poublanc, A. Crawley, D. Mandell, J. S. Han, M. Tymianski, K. TerBrugge, J. a Fisher, and D. J. Mikulis. Quantification of cerebrovascular reactivity by blood oxygen level-dependent MR imaging and correlation with conventional angiography in patients with Moyamoya disease.. *AJNR. American journal of neuroradiology*. 2010, Vol. 31, No. 5, pp. 862–7.

[65] Zaca, Domenico, Jun Hua, and Jay J. Pillai. Cerebrovascular reactivity mapping for brain tumor presurgical planning. *WJCO*. 2011, Vol. 2, No. 7, pp. 289-298.

[66] Fierstra, J., O. Sobczyk, A. Battisti-Charbonney, D. M. Mandell, J. Poublanc, A. P. Crawley, D. J. Mikulis, J. Duffin, and J. A. Fisher. Measuring cerebrovascular reactivity: what stimulus to use?. *The Journal of physiology*. 2013, Vol. 591, No. Pt 23, pp. 5809–21.

[67] Nakada, Kazuyoshi, Daisuke Yoshida, Mitsutaka Fukumoto, and Shoji Yoshida. Chronological analysis of physiological T2* signal change in the cerebrum during breath holding. *Journal of Magnetic Resonance Imaging*. 2001 , Vol. 13, No. 3, pp. 344-351.

[68] Leoni, R.F., K.C. Mazzeto-Betti, b K.C.Andrade, and D.B. de Araujoa. Quantitative evaluation of hemodynamic response after hypercapnia among different brain territories by fMRI. *Neuroimage*. 2008, Vol. 41, pp. 1192-1198.

[69] Kastrup, Andreas, Gunnar Krüger, Tobias Neumann-Haefelin, Gary H. Glover, and Michael E. Moseley. Changes of Cerebral Blood Flow Oxygenation and Oxidative Metabolism during Graded Motor Activation . *NeuroImage* . 2002, Vol. 15, No. 1, pp. 74-82.

[70] Tancredi, Felipe B, and Richard D Hoge. Comparison of cerebral vascular reactivity measures obtained using breath-holding and CO2 inhalation.. *Journal of cerebral blood flow and metabolism*. Nature Publishing Group, 2013, Vol. 33, pp. 1066–74.

[71] Prisman, Eitan, Marat Slessarev, Jay Han, Julien Poublanc, Alexandra Mardimae, Adrian Crawley, Joseph Fisher, and David Mikulis. Comparison of the effects of independently-controlled end-tidal PCO(2) and PO(2) on blood oxygen level-dependent (BOLD) MRI.. *Journal of magnetic resonance imaging : JMRI*. 2008, Vol. 27, No. 1, pp. 185–91.

[72] Stillman, a. E., X. Hu, and M. Jerosch-Herold. Functional MRI of Brain During Breath Holding at 4T. *Magnetic resonance imaging*. 1995, Vol. 13, No. 6, pp. 893–897.

[73] C.H., Moritz, Meyerand M.E., and Saykin A.J.. BOLD contrast response in human brain during simple breathhold measured at 1.5 Tesla. *In Proc., ISMRM, 6th Annual Meeting*. 1995, pp. 1405.

[74] Magon, Stefano, Alberto Beltramello, Gianpaolo Basso, Andrea Sbarbati, Paolo Farace, and Giuseppe Kenneth Ricciardi. Reproducibility of BOLD signal change induced by breath holding. *Neuroimage*. 2009, Vol. 25, pp. 702-712.

[75] Thomasona, Moriah E., and Gary H. Glovera. Controlled inspiration depth reduces variance in breath-holding-induced BOLD signal. *Neuroimage*. 2008, Vol. 39, pp. 206-214.

[76] Markus, H. S., and M. J. Harrison. Estimation of cerebrovascular reactivity using transcranial Doppler, including the use of breath-holding as the vasodilatory stimulus.. *Stroke; a journal of cerebral circulation*. 1992, Vol. 23, pp. 668–673.

[77] Bulte, Daniel P, Knut Drescher, and Peter Jezzard. Comparison of hypercapnia-based calibration techniques for measurement of cerebral oxygen metabolism with MRI.. *Magnetic resonance in medicine*. 2009, Vol. 61, No. 2, pp. 391–398.

[78] Birn, Rasmus M., Monica A. Smith, Tyler B. Jones, and Peter A. Bandettini. The respiration response function: The temporal dynamics of fMRI signal fluctuations related to changes in respiration. *Neuroimage*. 2008, Vol. 40, pp. 644-654.

[79] Simon, Aaron B, Valerie E M Griffeth, Eric C Wong, and Richard B Buxton. A Novel Method of Combining Blood Oxygenation and Blood Flow Sensitive Magnetic Resonance Imaging Techniques to Measure the Cerebral Blood Flow and Oxygen Metabolism Responses to an Unknown Neural Stimulus. *PLoS ONE*. 2013, Vol. 8, No. 1, pp. e54816.

[80] Liao, "C.H., K.J. Worsley, J.-B. Poline, J.A.D. Aston, G.H. Duncan, and A.C. Evans". "Estimating the Delay of the fMRI Response ". *"NeuroImage "*. "2002", Vol. "16", No. "3 Part A", pp. "593-606".

[81] Chang, Catie, Moriah E. Thomason, and Gary H. Glover. Mapping and correction of vascular hemodynamic latency in the BOLD signal. *Neuroimage*. 2008, Vol. 43, pp. 90-102.

[82] Blockley, Nicholas P, Ian D Driver, Susan T Francis, Joseph A Fisher, and Penny A Gowland. An improved method for acquiring cerebrovascular reactivity maps. *Magnetic Resonance in Medicine*. Wiley Subscription Services, Inc., A Wiley Company, 2011, Vol. 65, No. 5, pp. 1278–1286.

[83] Bright, Molly G., and Kevin Murphy. Reliable quantification of BOLD fMRI cerebrovascular reactivity despite poor breath-hold performance.. *NeuroImage*. Elsevier B.V., 2013, Vol. 83, pp. 559–68.

[84] *Moyamoya Disease*.
http://www.ninds.nih.gov/disorders/moyamoya/moyamoya.htm.

[85] *Alzheimer's Disease*.
http://www.ninds.nih.gov/disorders/alzheimersdisease/alzheimersdisease.htm.

[86] Mikulis, David J.. Chronic neurovascular uncoupling syndrome.. *Stroke; a journal of cerebral circulation*. 2013, Vol. 44, No. 6 Suppl 1, pp. S55–7.

[87] *Cerebral Aneurysms*.
http://www.ninds.nih.gov/disorders/cerebral_aneurysm/cerebral_aneurysms.htm.

[88] *Arterial Stenosis*.
http://www.ninds.nih.gov/disorders/stroke/arterial_stenosis_backgrounder.htm.

[89] Mandell, Daniel M., Jay S. Han, Julien Poublanc, Adrian P. Crawley, Jeff A. Stainsbyand, Joseph A. Fisher, and David J. Mikulis. Mapping Cerebrovascular Reactivity Using Blood Oxygen Level-Dependent MRI in Patients With Arterial Steno-occlusive Disease : Comparison With Arterial Spin Labeling. *Stroke*. 2008, Vol. 39, pp. 2021-2028.

[90] Njemanze, PC, OJ Beck, CR Gomez, S Horenstein, B Cujec, P Polasek, C Voll, A Shuaib, RJ Lee, T Bartzokis, and others. North American Symptomatic Carotid Endarterectomy Trial. Methods, patient characteristics, and progress.. *Stroke*. Am Heart Assoc, 1991, Vol. 22, No. 6, pp. 711–20.

[91] Penny, William D., Karl J.Friston, John T. Ashburner, Stefan J. Kiebel, and Thomas E. Nichols. *Statistical Parametric Mapping: The Analysis of Functional Brain Images: The Analysis of Functional Brain Images*. Academic Press, 2011.

[92] Ashburner, John, Gareth Barnes, and others. *SPM8 Manual – The FIL Methods Group*. Functional Imaging Laboratory, Wellcome Trust Centre for Neuroimaging, 2013.